Modeling Superconductors using Surface Impedance Techniques

by

Diana Prado Lopes Aude

Submitted to the Department of Physics in partial fulfillment of the requirements for the
Degree of

BACHELOR OF SCIENCE
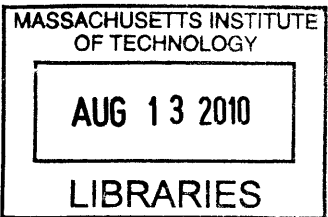
at the

MASSACHUSETTS INSTITUTE OF TECHNOLOGY

June 2010

© Diana Aude, 2010
All Rights Reserved

The author hereby grants to MIT permission to reproduce and to distribute publicly paper and
electronic copies of this thesis document in whole or in part.

Author_____
Department of Physics
21st of May 2010

Certified by_____
Professor Karl K. Berggren
Thesis Supervisor, Department of Electrical Engineering and Computer Science

Accepted by_____
Professor David E. Pritchard
Senior Thesis Coordinator, Department of Physics

Modeling Superconductors using Surface Impedance Techniques

by

Diana Prado Lopes Aude

Abstract

This thesis develops a simulation tool that can be used in conjunction with commercially available electromagnetic simulators to model the behavior of superconductors over a wide range of frequencies. This simulation method can be applied to metals both in the normal and superconducting state and is based on calculating surface impedance as a function of temperature, frequency and material parameters (such as the coherence length and the normal state conductivity). The surface impedance calculations apply the Mattis Bardeen and Zimmermann formulations of conductivity for superconductors to classical transmission line theory. When the tool is used with the Zimmermann formulation, it can model the behavior of superconductors with arbitrary purity, including very clean superconductors, which cannot be handled correctly by the Mattis Bardeen conductivity approach used in current simulators such as *SuperMix* [1].

Simulations were performed using the developed tool with Ansoft's HFSS EM simulator. The results for a copper printed circuit board resonator showed very good agreement with measured data, attesting to the soundness of the transmission line theory used to develop this tool. A microfabricated niobium coplanar waveguide resonator - for use in quantum computing applications - was also modeled and simulations gave the expected results for the electric field distributions and the variation of Q with temperature and capacitive coupling.

The tool developed here can therefore be used to predict the electromagnetic behavior of a superconducting device as function of the material parameters, operating temperature and frequency. With measurements of the device's Q at a recorded frequency and temperature, this tool can also be used to determine the mean free path of the material (assuming other material parameters such as coherence length, transition temperature (T_c) and the ratio of the energy gap to $k_B T_c$ are known). Equivalently, if all material parameters are known, comparison of Q measurements with simulation results can be used to determine the operating temperature, which may otherwise be difficult to measure in cryogenic environments.

Thesis supervisor: Karl K. Berggren
Title: Professor of Electrical Engineering

Acknowledgements

I would like to thank Prof. Karl Berggren for all his guidance, advice and instruction and for giving me the opportunity to work on this project. I've worked in Prof. Berggren's group since sophomore year and have always enjoyed being surrounded by such a dynamic and motivated group of people. Many thanks to Prof. Terry Orlando, for taking the time to meet with me many times to discuss superconductivity and for shedding light on so many concepts that were central to this thesis, such as the issue of locality in theories of conductivity. A special thanks to Prof. David Tait, for encouraging me throughout this whole project and for sharing his vast knowledge about transmission lines and quality factors. Many thanks to Adam McCaughan for introducing me to HFSS simulations, for fabricating the resonators and for being a great teammate. Thanks to Stephan Schulz for his guidance at the start of this project and for discussing atomic physics with me. Thanks to Prof. Todd Kemp for discussing methods of numerical integration with me and for his encouragement since freshman year. To my mother, who has always inspired me and believed in me, thank you so much for always being my best friend. And to my father, who I know is watching over me, this thesis is for you.

Contents

List of Figures

List of Tables

1 Introduction

Applications of superconductivity are becoming increasingly widespread in science and engineering. Low losses and high quality factors (Q factors) make superconducting cavities ideal for use as high efficiency detectors and resonators. In order to design and optimize such devices without resorting to an exhaustive repetition of fabrication and measurement cycles, we require an accurate simulation tool that, given a set of material parameters, can model superconducting behavior at a wide range of operating temperatures and frequencies. This thesis will develop such a tool from classical transmission line theory and the Mattis Bardeen and Zimmermann formulations of conductivity for superconductors. The functionality developed here can be applied to any electromagnetic simulation software package, and its use will be demonstrated with Ansoft's HFSS 3D full-wave electromagnetic field simulator.

The simulations presented here will contribute to the development of a quantum computer with molecular ions as qubits. We would like to use the two lowest rotational states of SrCl$^+$ molecular ions as |0> and |1> qubit states. The ions will be trapped in a microfabricated planar Paul trap [2] operated at cryogenic temperatures [3] with an integrated microwave stripline resonator which will deliver the 6.5GHz microwave radiation required to excite transitions between the two qubit states. The resonator takes a grounded coplanar waveguide (CPW) design and will act much like an optical cavity, trapping photons of the desired resonant frequency.

In order to do quantum computing with this system, we must be able to coherently manipulate the ions, and this manipulation requires a strong coupling between the field generated by the resonator and the microwaves emitted and absorbed by the ions: we would like spontaneous emission to occur into a single mode of the electromagnetic field and, since

probability of emission into a mode is proportional to occupation number, the resonator must trap a large number of photons in a single field mode. This translates into the requirement for a very high Q factor, which calls for the use of superconductors: a patterned layer of niobium, sputtered onto the top surface of the dielectric during fabrication, is expected to give rise to a thousand-fold increase in the Q factor below T_c.

Chapter 2 discusses the skin depth effect in normal metals and the surface impedance as a method of modeling real conductors. Chapter 3 extends the surface impedance treatment to superconductors using the Zimmermann and Mattis Bardeen conductivities, which are derived from the BCS (Bardeen-Cooper-Schrieffer) theory of superconductivity. Chapter 4 outlines the MATLAB routines developed from the theory in the first two chapters to calculate the surface impedance of a superconductor as a function of temperature, frequency and material parameters and presents simulation results for a copper printed circuit board resonator and for the niobium grounded CPW resonator described above.

2 Modeling Real Conductors

The challenge in modeling conductors under time varying excitations is that AC fields will permeate the surface of any real conductor and generate non-uniform current distributions, the simulation of which would require the time consuming solution of Maxwell's equations inside the conductor. A perfect conductor would present no such challenge, since there is no electric field in its interior and it can be modeled simply as a short circuit boundary. Similarly, a real conductor excited by a DC field needs only be represented by a resistive boundary since the current distribution within it will be uniform and will be completely defined by its resistivity and Ohm's law. We seek an analogous boundary condition for real conductors at AC, where the situation is complicated by the skin effect: a time-varying tangential electric field impinging on a real conductor will decay exponentially with distance from the surface, reaching $1/e$ of its value at the skin depth δ:

$$\delta = \sqrt{\frac{1}{\pi f \mu \sigma}} \qquad (2\text{-}1)$$

where f is the frequency of the impinging field; μ is the magnetic permeability and σ is the DC conductivity of the conductor. The boundary condition we require is given by the *surface impedance*, which is the impedance seen by the impinging electric field. The surface impedance in ohms/square is defined as the ratio of the voltage drop across an arbitrary length l along the surface of the conductor to the current enclosed by a square of area l^2 at the surface.

In this chapter, we will model the skin effect in a real conductor by a lumped-element circuit model. Following Kerr [4], we will use this model to derive the surface impedance of a conductor of both infinite (bulk) and finite thickness and we will discuss how to use this

boundary condition in ElectroMagnetic (EM) simulators. Finally, we will introduce the anomalous skin effect, which occurs at very low temperatures and high frequencies, when the behavior of charge carriers becomes dependent on non-local electric fields and the traditional Ohm's law is no longer valid.

2.1 Surface Impedance of a Thick Conductor

It will be useful to recall here that an infinitesimal length of a transmission line can be modeled by a lumped element circuit model as shown in Figure 2-1, where the resistance R is due to the resistivity of the real conductors which form the line, the inductance L arises from their self inductance, the conductance G represents dielectric losses and the capacitance C arises from the proximity of the two conductors [5].
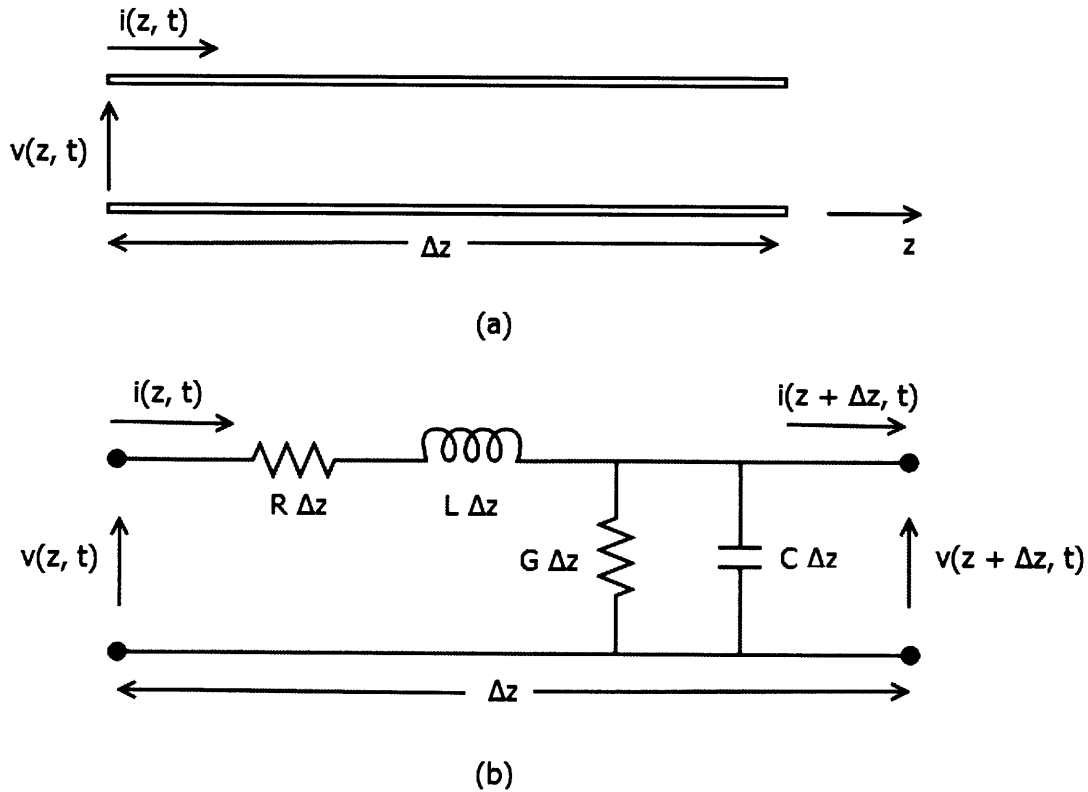
Figure 2-1 Infinitesimal length Δz of a transmission line (a) represented as a lumped element circuit model (b). The line is formed by two conductors separated by a dielectric (Figure redrawn from [5]).

We will now model the penetration of an electric field into a real conductor by viewing the conductor as a transmission line. Let us begin by analyzing the scenario depicted in Figure 2-2, where a plane wave is normally incident upon the surface of a thick conductor. Since the conductor is very thick, the surface impedance Z_s, seen by the wave incident at the surface of the conductor should be the same as that seen at a depth dz from the surface. We can therefore model the conductor as a transmission line with a section representing the sheet of infinitesimal thickness dz and terminated by an impedance Z_s.
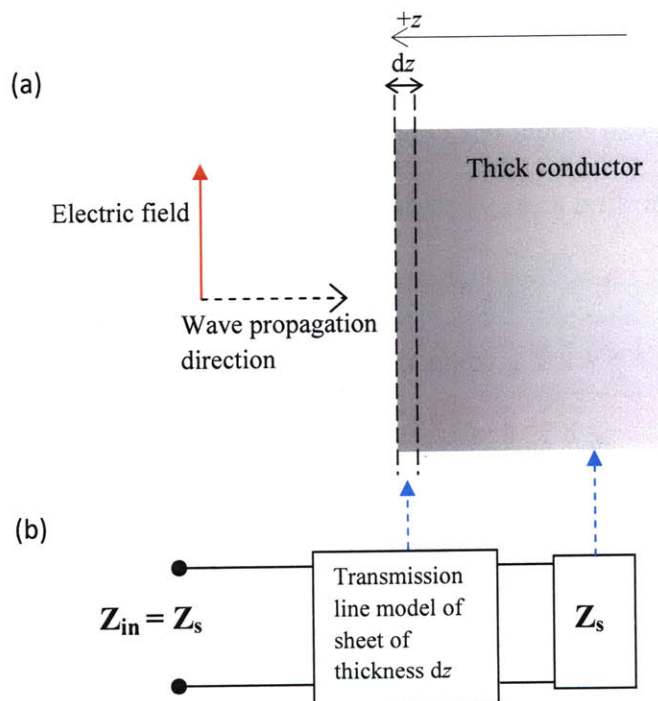
Figure 2-2: (a) Plane wave normally incident upon surface of a thick conductor. (b)This scenario can be modeled as transmission line with a section representing a thin sheet of thickness dz at the surface and terminated by an impedance Z_s, which represents the rest of the conductor and is the same as the impedance seen at the surface.

If we apply the transmission line circuit model of Figure 2-1 to this thin sheet, it is clear that the capacitance C does not apply since our transmission line consists of solid metal and, in the absence of a dielectric, charge separation is not possible. The resistance R can also be

neglected since the sheet is infinitesimally thin and the wave propagating into it will feel a vanishing resistance in the z direction. The conductance G, however, cannot be ignored since it is given by the conductivity of the sheet as experienced by current flowing parallel to the surface of the conductor, along the electric field direction: $dG = \sigma dz$ S/square, where σ is the conductivity of the metal in S/m. Finally, the inductance L will reflect the time delay introduced by the passage of the wave through this sheet: the wave will take a finite time to move from the surface to a depth dz because it propagates by accelerating electrons and, since this is a real conductor with finite conductivity, the electrons will take finite time to be accelerated. This inductance is derived from Ampere's law [4] to be $dL = \mu dz$ H/square.

With this, we can model our conductor with the lumped element circuit model shown in Figure 2-3, and use it to find an expression for Z_s.
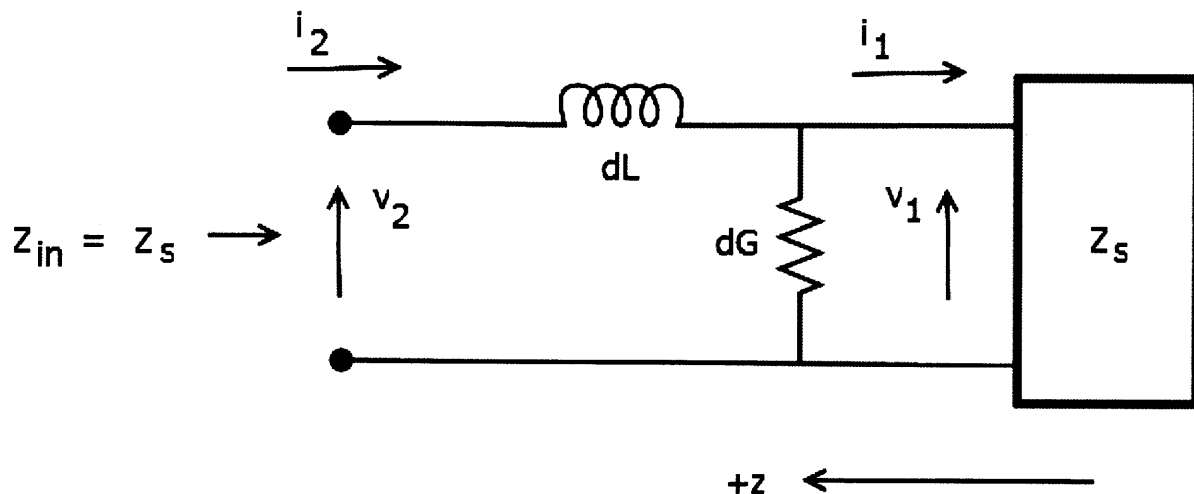
Figure 2-3: Lumped element circuit model for a real, thick conductor with surface impedance Z_s (Figure redrawn from [4])

From Figure 2-3, we have that:

$$Z_{in} = Z_s = j\omega dL + \cfrac{1}{dG + \cfrac{1}{Z_s}} = j\omega\mu dz + \cfrac{1}{\sigma dz + \cfrac{1}{Z_s}}$$

which implies that

$$Z_s^2 = j\omega\mu dz Z_s + \frac{Z_s^2}{\sigma Z_s dz + 1}$$

$$Z_s^2 = \frac{j\omega\mu}{\sigma}(\sigma Z_s dz + 1)$$

Now ignoring the terms in dz: $Z_s^2 = \frac{j\omega\mu}{\sigma}$, which gives:

$$\boxed{Z_s = (1+j)\sqrt{\frac{\omega\mu}{2\sigma}}}$$

(2-2)

2.2   Surface Impedance of a Conductor of Finite Thickness

One may be concerned that the model we have just constructed might not be useful in most engineering applications for two reasons: we will usually wish to model transmission lines, where the electric field is not normally incident upon the conductor, but instead travels along it; and we are often concerned with simulating thin conductors, or conductors with a finite thickness t. The first concern is immediately dismissed by [6], who shows that the field analysis of parallel propagation of a wave along the conductor yields the same solutions and surface impedance as that of the normal incidence scenario. The second concern is only really valid when the thickness is of the order of, or smaller than, the skin depth of the metal. This section will address this situation by using a slightly modified version of the circuit model presented in Section 2.1.

Here we will outline the derivation presented in [4], which begins by using the model of an infinitesimally thin sheet of thickness dz shown in Figure 2-4(a) to find an expression for the current at any depth z in the metal, $i(z)$. Note now that, if the wave is incident at $z = t$, where t is the thickness of the conductor, it will meet a second conductor-air interface at $z = 0$. As shown in Figure 2-4, this interface can be modeled by terminating the line with an impedance $Z_\eta = \sqrt{\frac{\mu_0}{\varepsilon_0}}$,

17

which is the impedance of free space [5]. Using the expression for $i(z)$ and this model, we can deduce the surface impedance by simply finding the ratio of the voltage at the surface, $v(t)$ to the current at the surface, $i(t)$, which Kerr [4] determines to be:
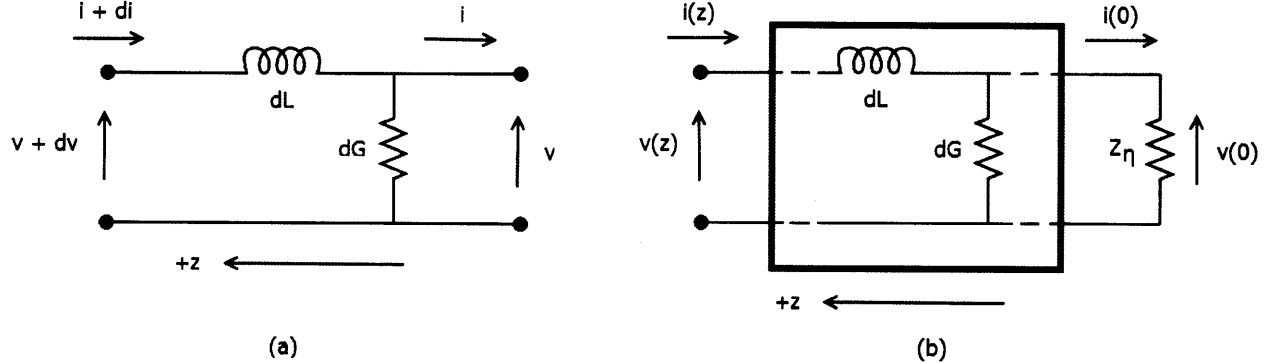
Figure 2-4: (a) Circuit model of sheet of thickness dz. (b) Circuit model of conductor-air interface. (Figure redrawn from [4])

$$Z_S = \frac{v(t)}{i(t)} = \frac{k}{\sigma}\left[\frac{e^{kt} + \frac{\sigma Z_\eta - k}{\sigma Z_\eta + k}e^{-kt}}{e^{kt} - \frac{\sigma Z_\eta - k}{\sigma Z_\eta + k}e^{-kt}}\right] \qquad (2\text{-}3)$$

with $k = \frac{(1+j)}{\delta}$.

But note that for applications of interest, frequencies are in the Gigahertz range and metals used are very good conductors so that ω is on the order of 10^9 radians/s, $\sigma \sim 10^7$ S/m, so that:

$$\frac{k}{\sigma} = (1+j)\sqrt{\frac{\omega\mu}{2\sigma}} \Rightarrow \left|\frac{k}{\sigma}\right| \sim 10^{-2}\Omega,$$

while $Z_\eta = \sqrt{\frac{\mu_0}{\varepsilon_0}} \approx 377\Omega.$

Therefore, Z_η is about 4 orders of magnitude greater than $\frac{k}{\sigma}$, which allows us to write:

$$\frac{\sigma Z_\eta - k}{\sigma Z_\eta + k} = \frac{Z_\eta - \frac{k}{\sigma}}{Z_\eta + \frac{k}{\sigma}} \approx 1,$$

and equation (2-3) reduces to:

$$Z_S = \frac{k}{\sigma}\left[\frac{e^{kt} + e^{-kt}}{e^{kt} - e^{-kt}}\right] = \frac{k}{\sigma}\coth(kt). \qquad (2\text{-}4)$$

18

2.3 Using Surface Impedance to Model Conductors in EM Simulators

The effect of a real conductor on an EM wave travelling in air can now be entirely captured by the simple transmission line model shown in Figure 2-5: a line of characteristic impedance Z_η terminated by the surface impedance of the conductor Z_s, which can be calculated as shown in sections 2.1 and 2.2.
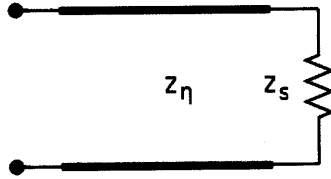
Figure 2-5: Transmission line model for EM wave incident upon a real conductor.

We now require a feasible way to implement this model in EM simulators, such Ansoft's HFSS. Using a single boundary with the correct surface impedance to represent a metal sheet would work, but it would be useful to preserve the geometry and dimensionality of the structure we are modeling. Kerr [4] suggests representing the conductor as two sheets of the appropriate surface impedance, separated by the thickness t. He finds that the surface impedance of each sheet will have to be slightly modified from Z_s and here we will use transmission line theory to prove his result and suggest a generalized form of his correction.

From Figure 2-6, we see that free space between the two sheets of impedance Z_s can be modeled as the transmission line shown in (b). It is well known from transmission line theory [5] that, for a lossless transmission line of length t with characteristic impedance Z_η terminated by a load Z_s, the impedance looking into the line is:

$$Z_{in} = Z_\eta \frac{Z_s + jZ_\eta \tan(\beta t)}{Z_\eta + jZ_s \tan(\beta t)},$$

(2-5)

Where $\beta = \beta_0 = \omega \sqrt{\mu_0 \varepsilon_0} = \frac{\omega}{c} = \frac{2\pi}{\lambda}$.

(2-6)

19
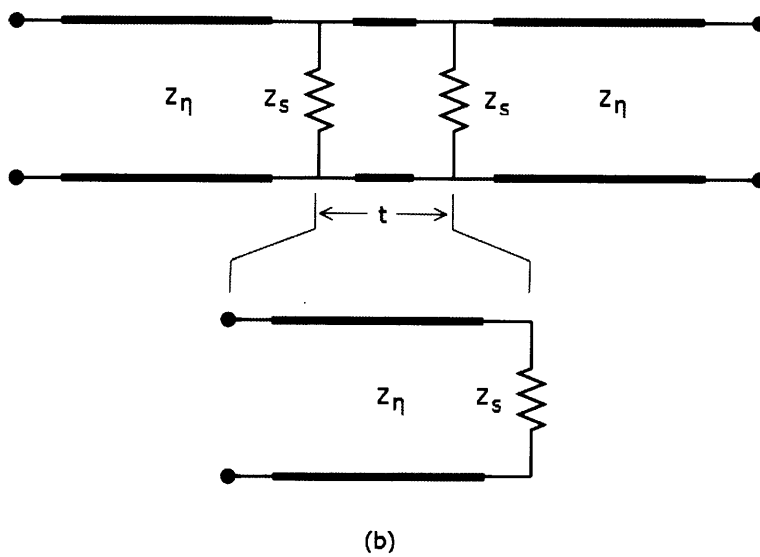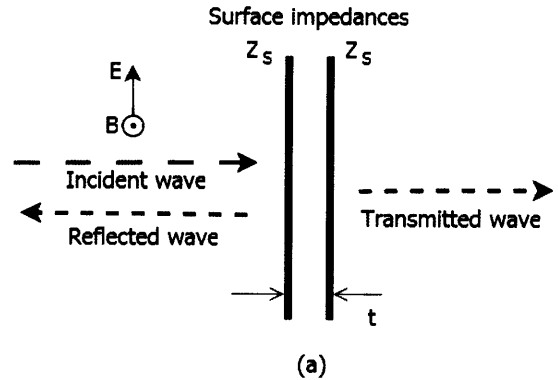
Figure 2-6: (a) Two-sheet model for a finite thickness conductor. (b) Transmission line circuit model of (a) – the transmission line between the two sheets is highlighted as a line of length t, characteristic impedance Z_η and load Z_s. (Figure modified and redrawn from [4])

We know that the impedance of free space is much greater than the surface impedance of a conductor, so we have that:

$$Z_\eta \gg Z_s \ \Rightarrow \ \frac{Z_s}{Z_\eta} \ll 1.$$

Dividing top and bottom of equation (2-5) by Z_η:

$$Z_{in} \approx Z_s + jZ_\eta \tan(\beta t), \qquad\qquad (2\text{-}7)$$

so the transmission line will look like a load Z_s in series with an inductor with inductance

$L_t = \frac{Z_\eta \tan{(\beta t)}}{\omega}$ as shown in Figure 2-7 (a). For thin films with $t \ll \lambda$, βt will be small and we see

from equation (2-6) that L_t reduces to: $L_t^{t \ll \lambda} \approx \frac{Z_\eta \beta t}{\omega} \approx \sqrt{\frac{\mu_0}{\varepsilon_0}}\sqrt{\mu_0 \varepsilon_0}\, t = \mu_0 t$, which is the result

obtained by Kerr [4].
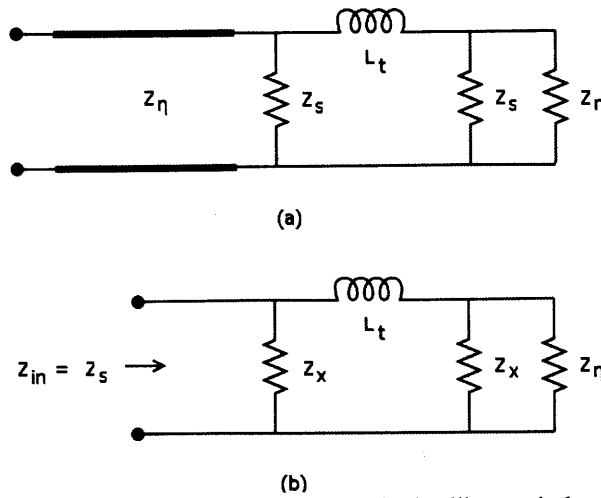
Figure 2-7: (a) The transmission line between the two sheets looks like an inductance L_t. (b) We can find the impedance Z_X which corrects for the effect of this inductance by setting $Z_{in} = Z_s$. (Figure modified and redrawn from [4])

As in Figure 2-7 (b), we can correct for the effect of L_t by finding the impedance Z_X

which makes $Z_{in} = Z_s$. Noting that Z_η is large and can be approximated as an open circuit, one

finds that the impedance of each of the sheets representing the conductor should be set to:

$$Z_X = \frac{1}{2}\left[(2Z_s - j\omega L_t) \pm [4Z_s^2 + (j\omega L_t)^2]^{\frac{1}{2}}\right] \qquad (2\text{-}8)$$

which is applicable for any thickness t and is a more general version of the correction given by

Kerr, which sets $L_t = \mu_0 t$ and is to be used only when $t \ll \lambda$.

2.4 The Anomalous Skin Effect and NonLocality

In deriving the surface impedance of a conductor, we used a transmission line analogy which implicitly assumed that the familiar Ohm's law, $J = \sigma E$, held i.e. that current density J at a certain point inside the conductor would depend only on the electric field E at that point in space and at that moment in time. However, it has been observed that, both at very low temperatures and at very high frequencies, the measured surface resistance is much higher than that predicted by the normal skin effect theory [6]. The low temperature effect, named the anomalous skin effect, is attributed to the fact that Ohm's law ceases to be valid locally and the current density at a given point depends on the electric fields in a surrounding volume of metal. At high frequencies, the phenomenon is named the extreme anomalous effect and occurs because the electric field changes fast enough for electrons to feel this change between scattering events, causing their velocities to become dependent upon previous states. In this section, we explore the origin of these nonlocal effects and attempt to give a more quantitative notion of when they occur.

The crucial point is that the usual derivation of Ohm's law from the free electron theory of metals, as given for instance in [7], assumes that the electric field seen by an electron between scattering events is *constant* and gives a linear relationship between the current density and the electric field at a point r in the metal:

$$J(r) = \frac{\sigma_{dc}}{1 + j\omega\tau} E(r)$$

Where σ_{dc} is the DC conductivity of the metal and $\tau = \frac{l}{v_f}$ is the relaxation time of the electrons, given by the ratio of the mean free path l to the Fermi velocity v_f.

The skin depth δ is the smallest electromagnetic length scale in our problem: if it is much larger than the mean free path, it is clear that the electrons will not see significant variation in the field between scatters. But l increases with decreasing temperature - since fewer lattice vibrations translate into a longer mean free path – and therefore, at very low temperatures or very high frequencies (i.e. small δ by (2-1)), l becomes of the same order of magnitude of δ. In this scenario, the current density at r will depend upon an average of the electric field over a sphere of radius l around r. This non-local version of Ohms Law was derived by Reuter and Sondheimer and can be written as [6]:

$$J(r,t) = \frac{3\sigma_{dc}}{4\pi l} \int \frac{r(r \cdot [E])e^{-r/l}}{r^4} dV$$

where r is the distance from the origin in meters, l is the mean free path and $[E]$ is the electric field at volume dV at a time $t - r/v_f$, where v_f is the electron velocity at the Fermi surface (i.e. the retarded field).

In the non-local limit, equation (2-4) for the surface impedance of a normal conductor is no longer valid. However, since we are working with microwave frequencies, our skin depths will be of the order microns, while the mean free path of an electron in a very good conductor at room temperature will be of the order of nanometers, so here we are safely in the local limit. In dealing with superconductors however, we must also concern ourselves with checking whether or not we can assume local relationships in deriving surface impedance, and we will address this issue in the next chapter.

3 Modeling Superconductors

3.1 The Length Scales of Superconductivity

In 1957 Bardeen, Cooper and Schrieffer developed a theory of superconductivity [8] which postulated that electrons in a superconductor can attract each other by coupling to lattice phonons. As explained by Kittel [7], this interaction occurs because, as an electron moves through a lattice of positive ions, it will attract nearby ions, causing the lattice to deform around it. A second electron will then move to lower its potential energy in the deformed lattice, thus becoming indirectly attracted to the first electron. This attraction leads to a correlation between pairs of electrons of opposite spin and momentum, named Cooper pairs: in a superconductor, either both the orbital $k\uparrow$ with wavevector k and spin up and the orbital $-k\downarrow$ with wavevector $-k$ and spin down are occupied, or both these orbitals are vacant [7]. This implies that however the $k\uparrow$ electron scatters, the same scattering will be mirrored in the $-k\downarrow$ electron, so that the overall change in momentum of the electron gas is zero – this translates into the macroscopic effect of zero DC electrical resistance. In the superconducting regime, a metal will be characterized by the following parameters:

- *Energy gap at zero temperature, Δ_0*: A Fermi gas of noninteracting electrons allows for arbitrarily small excitations, since an electron can be excited to a state at any small energy above the Fermi surface. In a superconductor, however, BCS theory predicts an energy gap between the ground state and the excited states. For niobium, BCS theory gives a gap ratio of $\frac{\Delta_0}{k_B T_c} = 1.76$, where T_c is the transition temperature of the superconductor and k_B is Boltzmann's constant. This ratio varies slightly from the BCS value in the literature due to strong coupling effects, whereby the electrons and phonons

25

couple more strongly than predicted by BCS theory [9]. Some quoted values of gap ratios for niobium are given in Table 3-1.

- *Intrinsic coherence length* ξ_0: The coherence length is a measure of the distance over which the correlation between electron pairs persists in a superconductor and is given by:

$$\xi_0 = \frac{\hbar v_f}{\pi \Delta_0}$$

where $\hbar$ is the reduced Planck's constant and v_f is the electron velocity at the Fermi surface. We will see in this chapter that the intrinsic coherence length is a key parameter in determining the volume over which we have to integrate the magnetic vector potential to obtain the current density in a superconductor – its relationship to other characteristic length scales of a superconductor will determine whether or not this integration can be reduced to a local Ohm's law relationship.

- *London penetration depth* $\lambda_{L,0}$ *and BCS effective penetration depth* $\lambda_{\mathrm{eff}}(T)$: The penetration depth is a measure of the depth of penetration of the magnetic field in superconductors. The London penetration depth at zero temperature $\lambda_{L,0}$ is derived from the London equations, which arise from a simplified phenomenological theory of superconductivity that is approximates well the behavior of clean (with mean free path approaching infinity) superconductors in the local regime [10]. Linden [9] gives an approximate relationship between the BCS penetration depth $\lambda_{\mathrm{eff}}(T)$ and the London depth $\lambda_{L,0}$:

$$\lambda_{\mathrm{eff}}^2(T) = \frac{\lambda_{\mathrm{eff}}^2(0)}{\left[1-\left(\frac{T}{T_c}\right)^{3-\frac{T}{T_c}}\right]} \quad , \quad \lambda_{\mathrm{eff}}^2(0) = \lambda_{L,0}\left(1+\frac{\xi_0}{l}\right)^{1/2} \tag{3-1}$$

We will see in this chapter that these parameters, along with the mean free path l and the superconducting transition temperature T_c, define the behavior of a superconductor and determine the method by which we can calculate its surface impedance.

3.2   The Mattis Bardeen Conductivity

In 1958 Mattis and Bardeen [10] used BCS theory to derive the following expression relating the current density $J(r)$ and the magnetic vector potential $A(r)$ [11]:

$$J(r) = \frac{3}{4\pi^2 v_f \hbar \lambda_{L0}^2} \int_V \frac{R \cdot R \cdot A(r')I(\omega,R,T)e^{-\frac{R}{l}}}{R^4} dr' \tag{3-2}$$

where we have defined the magnetic vector potential as $H(r) = \nabla \times A(r)$, $R = r - r'$, v_f is the Fermi velocity of the electrons, λ_{L0}^2 is the London penetration depth at zero temperature, and

$$I(\omega,R,T) = -j\pi \int_{\Delta-\hbar\omega}^{\Delta} [1 - 2f(E + \hbar\omega)][g(E)\cos(\alpha\Delta_2) - j\sin(\alpha\Delta_2)]e^{j\alpha\Delta_1}dE$$

$$-j\pi \int_{\Delta}^{\infty} [1 - 2f(E + \hbar\omega)][g(E)\cos(\alpha\Delta_2) - j\sin(\alpha\Delta_2)]e^{j\alpha\Delta_1}dE$$

$$+j\omega \int_{\Delta}^{\infty} [1 - 2f(E)][g(E)\cos(\alpha\Delta_1) + j\sin(\alpha\Delta_1)]e^{-j\alpha\Delta_2}dE$$

with

$$\Delta_1 = \begin{cases} \sqrt{E^2 - \Delta^2}, |E| > \Delta \\ j\sqrt{\Delta^2 - E^2}, |E| < \Delta \end{cases}, \Delta_2 = \sqrt{(E + \hbar\omega)^2 - \Delta^2}, g(E) = \frac{E^2 + \Delta^2 + \hbar\omega E}{\Delta_1\Delta_2}, \alpha = R/(\hbar v_f)$$

where $\Delta = \Delta(T)$ is the energy gap at temperature T and $f(E)$ is the Fermi function given by:

$$f(E) = \frac{1}{1 + e^{\frac{E}{k_B T}}}$$

where k_B is the Boltzmann constant.

As noted by Gao [11], the function $I(\omega, R, T)$ decays with a characteristic length scale $R \sim \xi_0$ since the coherence length ξ_0 defines the distance over which the density of superconducting electrons remains approximately constant. Therefore, the function $I(\omega, R, T)e^{-R/l}$, will decay on a length scale given by the smaller of ξ_0 and l. So it is the smaller of ξ_0 and l of that will define the effective radius of the volume V over which we are integrating in (3-2) – outside this volume, the integral is negligible. If this radius is small compared to the effective penetration depth λ_{eff} of the penetrating magnetic field –i.e. the length scale over which the electromagnetism changes in the superconductor – the electrons will see a constant field and we are in a local regime: the magnetic vector potential $A(r')$ will be virtually constant over the volume of integration and can therefore be taken out of the integral. Equation (3-2) then reduces to:

$$J(r) = -K_0(\xi_0, l, T)A(r) \tag{3-3}$$

where $K_0(\xi_0, l, T)$ is a constant that depends on ξ_0, l and T, as shown by [11]. From Maxwell's equations, and recalling that here we have that $H = \nabla \times A = \dfrac{B}{\mu_0}$, we find:

$$E = -\nabla\phi - \mu_0\frac{\partial A}{\partial t},$$

but here we can set $-\nabla\phi = 0$ because, if ϕ were nonzero we would always have a constant electric field E_o (as well as the time-varying field due to $\frac{\partial A}{\partial t}$) in the metal and there is no such field here. So $E = -\mu_0\frac{\partial A}{\partial t}$ and, if we take A to be of the form $A(r,t) = A_o(r)e^{j\omega t}$, we have that $E = -j\mu_0\omega A$. From (3-2) we see that:

$$J = \frac{-K_0(\xi_0, l, T)}{j\mu_0\omega}E,$$

from which we now define the complex conductivity which was first proposed by Glover and Tinkham [12]:

$$\sigma_{MB} = \frac{-K_0(\xi_0, l, T)}{j\mu_0\omega}$$

And now we have returned to Ohm's Law with $J = \sigma_{MB}E$! This implies we are free to use the classical surface impedance formulae derived in Chapter 2, provided we substitute the normal conductivity for σ_{MB}. Mattis and Bardeen [10] give the following expressions for σ_{MB}:

Letting $\sigma_{MB} = \sigma_1 - j\sigma_2$:

$$\frac{\sigma_1}{\sigma_n} = \frac{2}{\hbar\omega}\int_{\Delta}^{\infty} \frac{[f(E) - f(E + \hbar\omega)](E^2 + \Delta^2 + \hbar\omega E)}{\sqrt{E^2 - \Delta^2}\sqrt{(E + \hbar\omega)^2 - \Delta^2}}dE$$

$$+ \frac{1}{\hbar\omega}\int_{\Delta - \hbar\omega}^{-\Delta} \frac{[1 - 2f(E + \hbar\omega)](E^2 + \Delta^2 + \hbar\omega E)}{\sqrt{E^2 - \Delta^2}\sqrt{(E + \hbar\omega)^2 - \Delta^2}}dE$$

(3-4)

$$\frac{\sigma_2}{\sigma_n} = \frac{1}{\hbar\omega}\int_{max\{\Delta - \hbar\omega, -\Delta\}}^{\Delta} \frac{[1 - 2f(E + \hbar\omega)](E^2 + \Delta^2 + \hbar\omega E)}{\sqrt{\Delta^2 - E^2}\sqrt{(E + \hbar\omega)^2 - \Delta^2}}dE$$

(3-5)

Where σ_n is the normal state conductivity and the second integral in equation (3-4) vanishes if $\hbar\omega < 2\Delta$.

A Matlab program, *supercond.m* (printed in Appendix A), was written to numerically evaluate the conductivity integrals. The program's output is the ratio of the Mattis Bardeen conductivity to the normal conductivity of a material at any frequency and temperature, and the only inputs it requires are the superconducting transition temperature T_c, and the energy gap at zero temperature Δ_0. Figure 3-1 plots the output of *supercond.m* for niobium at a range of values of frequency and temperature.
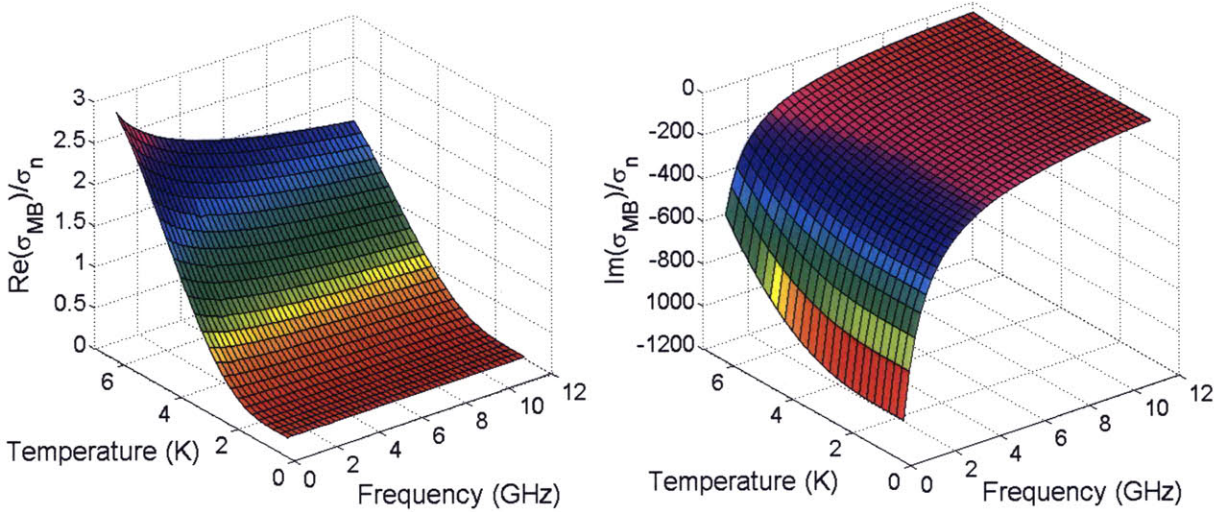
Figure 3-1: Plots of the real and imaginary parts of the ratio of the Mattis Bardeen conductivity to the normal conductivity of niobium for a range of values of temperature and frequency as calculated by the program *supercond.m*. Here, $T_c = 9.2K$ and $\frac{\Delta(0)}{k_B T_c} = 1.83$.

As given in equations (3-4) and (3-5), the conductivity integrals are singular since the square root terms in their denominators are zero at their upper or lower limits. To remove these singularities, we use the following substitutions:

To remove lower limit singularities:

$$\int_a^b \frac{F(E)}{\sqrt{E^2 - a^2}} dE \xrightarrow{E=a+x^2} 2\int_0^{\sqrt{b-a}} \frac{F(a+x^2)}{\sqrt{2a+x^2}} dx$$

To remove upper limit singularities:

$$\int_a^b \frac{F(E)}{\sqrt{b^2 - E^2}} dE \xrightarrow{E=b-x^2} 2\int_0^{\sqrt{b-a}} \frac{F(b-x^2)}{\sqrt{2b-x^2}} dx$$

In order to calculate the energy gap at temperature T, $\Delta = \Delta(T)$, the function *gapcond.m*, was adapted from a routine in the C++ software library *SuperMix* [1], a freely available software library for high-frequency circuit optimization and design. The routine linearly interpolates a table of values of $\Delta(T)$ measured by Mühlschlegel [13] to find the gap at any temperature.

SuperMix also contains a routine that calculates the Mattis Bardeen conductivity ratios for surface impedance calculations and the output of *supercond.m* was verified against this routine for temperature $T = 4.2$K and a frequency range of 0-12GHz. As shown in Figure 3-2, the two outputs were found to be identical.
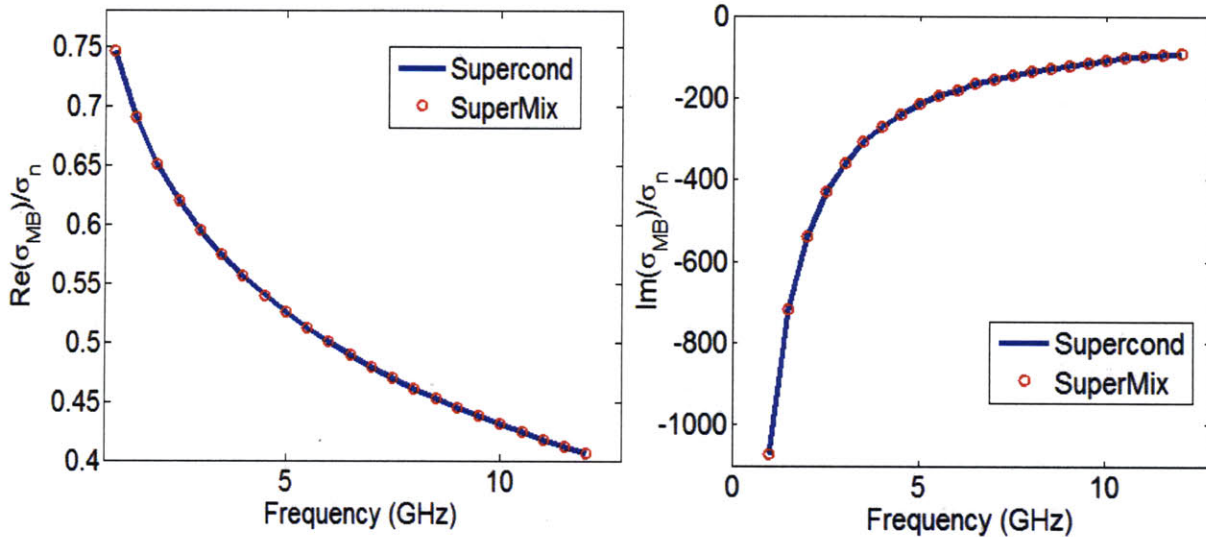
Figure 3-2: Comparison of the output of *supercond.m* and *SuperMix* for a temperature $T=4.2$K, $\Delta_0/k_BT_c = 1.9$[1] and a frequency range of 0-12GHz. The two programs output the same values.

It is important to remember that the Mattis Bardeen conductivity can only be used when $\xi_0 \ll \lambda_{\text{eff}}$ or $l \ll \lambda_{\text{eff}}$. Since the coherence length in a given superconductor is a fixed parameter (independent of frequency, temperature and purity), it is the mean free path l which will determine the applicability of the local limit of the Mattis Bardeen theory to a given sample. If the sample is dirty and l is very small compared to the effective penetration depth, the Mattis Bardeen conductivity will give a very good approximation of the actual behavior of the superconductor. However, as l increases and the material becomes cleaner, we will violate the $l \ll \lambda_{\text{eff}}$ condition and move away from the local limit of the theory – the use of the Mattis Bardeen conductivity will then no longer be appropriate. For such situations, we must either

---

[1] The agreement between *supercond* and supermix holds at any temperature T, over any frequency and for any any gap ratio $\Delta(0)/k_BT_c$ as long as the same parameters are fed into both programs. (*SuperMix* usually uses $\Delta(0)/k_BT_c=1.83$)

evaluate the full non-local Mattis Bardeen integral, or seek an alternative formulation of the theory which offers a simpler computation method for arbitrary sample purity. The next section will explore such an alternative.

3.3 The Zimmermann Conductivity

In 1991, Zimmermann [14] used energy integrated Green functions to derive an expression for the complex conductivity of a homogeneous isotropic BCS superconductor with arbitrary mean free path. He found that:

$$\sigma_{sc} = \frac{\sigma_0 j}{2\omega\tau} \times \left(J + \int_\Delta^\infty I_2 dE \right),$$

$$\text{for } J(\omega \le 2\Delta) = \int_\Delta^{\omega+\Delta} I_1 dE,$$

$$I_1 = \tanh\left(\frac{E}{2k_B T}\right) \left\{ \left[1 - \frac{\Delta^2 + E(E-\omega)}{P_4 P_2} \right] \frac{1}{P_4 + P_2 + \frac{j}{\tau}} - \left[1 + \frac{\Delta^2 + E(E-\omega)}{P_4 P_2} \right] \frac{1}{P_4 - P_2 + \frac{j}{\tau}} \right\},$$

$$I_2 = \tanh\left(\frac{E+\omega}{2k_B T}\right) \left\{ \left[1 + \frac{\Delta^2 + E(E+\omega)}{P_1 P_2} \right] \frac{1}{P_1 - P_2 + \frac{j}{\tau}} - \left[1 - \frac{\Delta^2 + E(E-\omega)}{P_1 P_2} \right] \frac{1}{-P_1 - P_2 + \frac{j}{\tau}} \right\}$$

$$+ \tanh\left(\frac{E}{2k_B T}\right) \left\{ \left[1 - \frac{\Delta^2 + E(E+\omega)}{P_1 P_2} \right] \frac{1}{P_1 + P_2 + \frac{j}{\tau}} - \left[1 + \frac{\Delta^2 + E(E-\omega)}{P_1 P_2} \right] \frac{1}{P_1 - P_2 + \frac{j}{\tau}} \right\},$$

$$I_3 = \tanh\left(\frac{E}{2k_B T}\right) \left\{ \left[1 - \frac{\Delta^2 + E(E+\omega)}{P_3 P_2} \right] \frac{1}{P_3 + P_2 + \frac{j}{\tau}} - \left[1 + \frac{\Delta^2 + E(E-\omega)}{P_3 P_2} \right] \frac{1}{P_3 - P_2 + \frac{j}{\tau}} \right\},$$

where:

$$P_1 = \sqrt{(E+\omega)^2 - \Delta^2}, P_2 = \sqrt{E^2 - \Delta^2}, P_3 = \sqrt{(E-\omega)^2 - \Delta^2}, P_4 = j\sqrt{\Delta^2 - (E+\omega)^2},$$

32

where $\hbar$ has been normalized to 1, σ_0 is the normal state conductivity and $\tau = \frac{l}{v_0}$ is the scattering time constant, given by the ratio of the mean free path to the Fermi velocity.

In [14], Zimmermann gives a FORTRAN program to calculate σ_{sc}/σ_0, which was translated here to a Matlab script *zimcond.m* (see Appendix A.2). The inputs to Zimmermann's program are: $x = \frac{\hbar\omega}{2\Delta}$, $y = \frac{\hbar}{2\Delta\tau}$ and $tt = \frac{T}{T_c}$,

but we can write, from [11]: $$\xi_0 = \frac{\hbar v_0}{\pi\Delta_0},$$

So that we have $$y = \frac{\hbar v_0}{2\Delta l} = \frac{\pi\xi_0\Delta_0}{2l\Delta}.$$

Therefore, the only parameters required to calculate σ_{sc} are $\xi_0, \Delta_0, \sigma_0$ and T_c. $\Delta(T)$ is again calculated here using the *gapcond.m* routine taken from *Supermix*, which interpolates Mühlschlegel's data [13] to find the gap at any temperature. Figure 3-3 uses *zimcond.m* to reproduce Zimmermann's results as plotted in Fig.1 of [14].
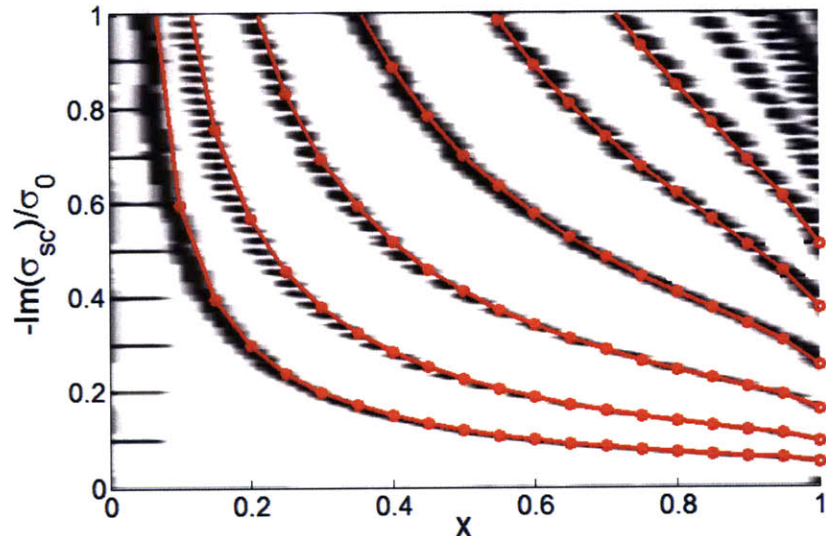

Figure 3-3: Verification of *zimcond.m* against Zimmermann's program: The black lines are taken from Fig.1. in [14], which plots the results of Zimmermann's program for input values of x from 0 to 1 and y from 0.0625 to 4. The overlaid red lines are the results produced by *zimcond.m* when given the same inputs.

We now have a conductivity which is applicable for any mean free path length, and we can plug
it into the classical surface impedance formulae derived in Chapter 2 to calculate the surface
impedance of niobium, as shown in Figure 3-4 .
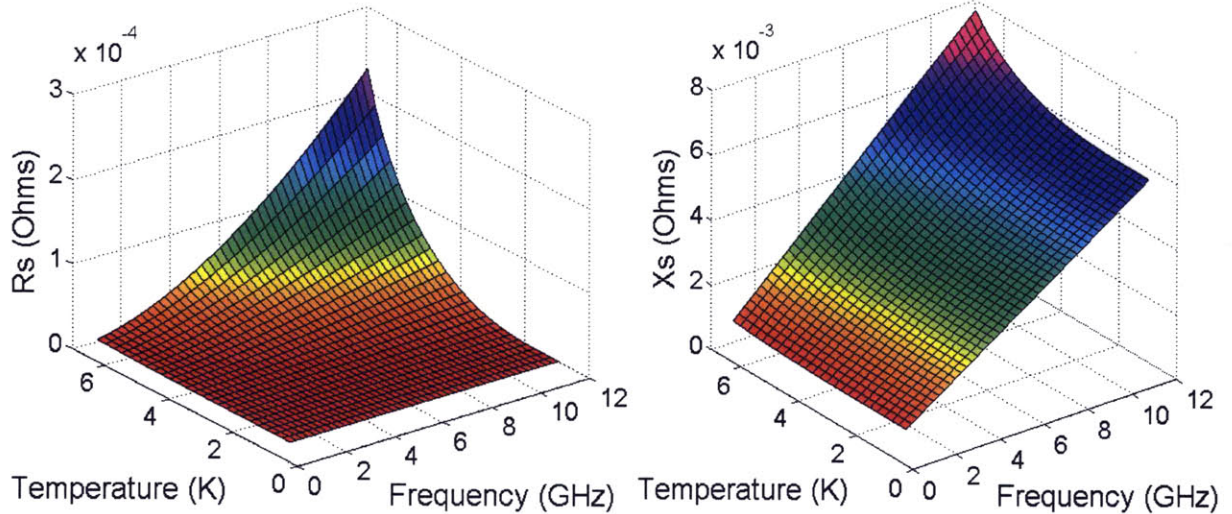
Figure 3-4: Bulk surface resistance R_s and surface reactance X_s over a range of frequencies and temperatures for
niobium. The plots were generated by using *zimcond.m* to calculate the Zimmermann conductivity, $\sigma_{sc}(\omega, T)$ and
then applying the classical formula for bulk surface impedance (2-2) with $\sigma_{sc}(\omega, T)$ in place of the normal
conductivity σ.

3.4   Comparison of the Zimmermann and Mattis Bardeen Conductivities

We would like to check the consistency of the Mattis Bardeen and Zimmermann theories.
Whilst the Zimmermann conductivity is applicable at any mean free path l, we found in
section 3.2 that the Mattis Bardeen conductivity is only valid when $\xi_0 \ll \lambda_{eff}$ or $l \ll \lambda_{eff}$. From
equation (3-1), we see λ_{eff} increases with decreasing mean free path l and that λ_{L0}, the London
penetration depth at zero temperature, is a lower bound for λ_{eff}. The values of λ_{L0} for niobium
vary in the literature: Gao [11] quotes it as 33 nm whilst Linden [15], for instance, takes it to be
29 nm. However, for all quoted values of λ_{L0} it is clear the condition $\xi_0 \ll \lambda_{L0}$ does not hold for
niobium, since $\xi_0 = 39$nm. Therefore, what will determine whether or not the Mattis Bardeen
conductivity is applicable for Niobium is its purity: very dirty niobium with very small values of

34

l will satisfy $l \ll \lambda_{\text{eff}}$, whilst clean niobium will fall into the non-local regime of the Mattis Bardeen theory.

We therefore expect the surface impedance as calculated from the Mattis Bardeen and Zimmermann conductivities to be equal for very dirty niobium, but to diverge as the niobium becomes cleaner. To check this, we consider in Table 3-1 three samples of niobium studied in the literature and calculate their mean free paths using the following equation from [9]:

$$\frac{l}{\xi_0} = \frac{\pi \Delta_0 \lambda_{L0} \sigma_0 \mu_0}{\hbar}$$
(3-6)

The parameters for the *"Dirty"* niobium listed in the last column of Table 3-1 are taken from *Supermix* [1], which uses the Mattis Bardeen conductivity to calculate surface impedance.

Parameters	*"Clean"* l=100nm	*"Mid-Range"* l=20nm	*"Dirty"* l=5.7nm
σ_o	3.3×10^8S/m	5.6×10^7S/m	2.0×10^7S/m
$\Delta(0)/k_B T_c$	1.97	1.76	1.83
λ_{L0}	29nm	33nm	29nm
ξ_0	39nm	39nm	39nm
T_c	9.2K	9.2K	9.2K
Source:	*Linden* [15]	*Gao* [11]	*SuperMix* [1]

Table 3-1: Parameter values for different niobium samples studied in the literature and their calculated mean free paths.

From Figure 3-5 we see that, just as expected, the Mattis Bardeen and Zimmermann conductivities yield very different surface impedances in the clean limit but produce very similar results as we approach the dirty limit – the two theories are consistent.
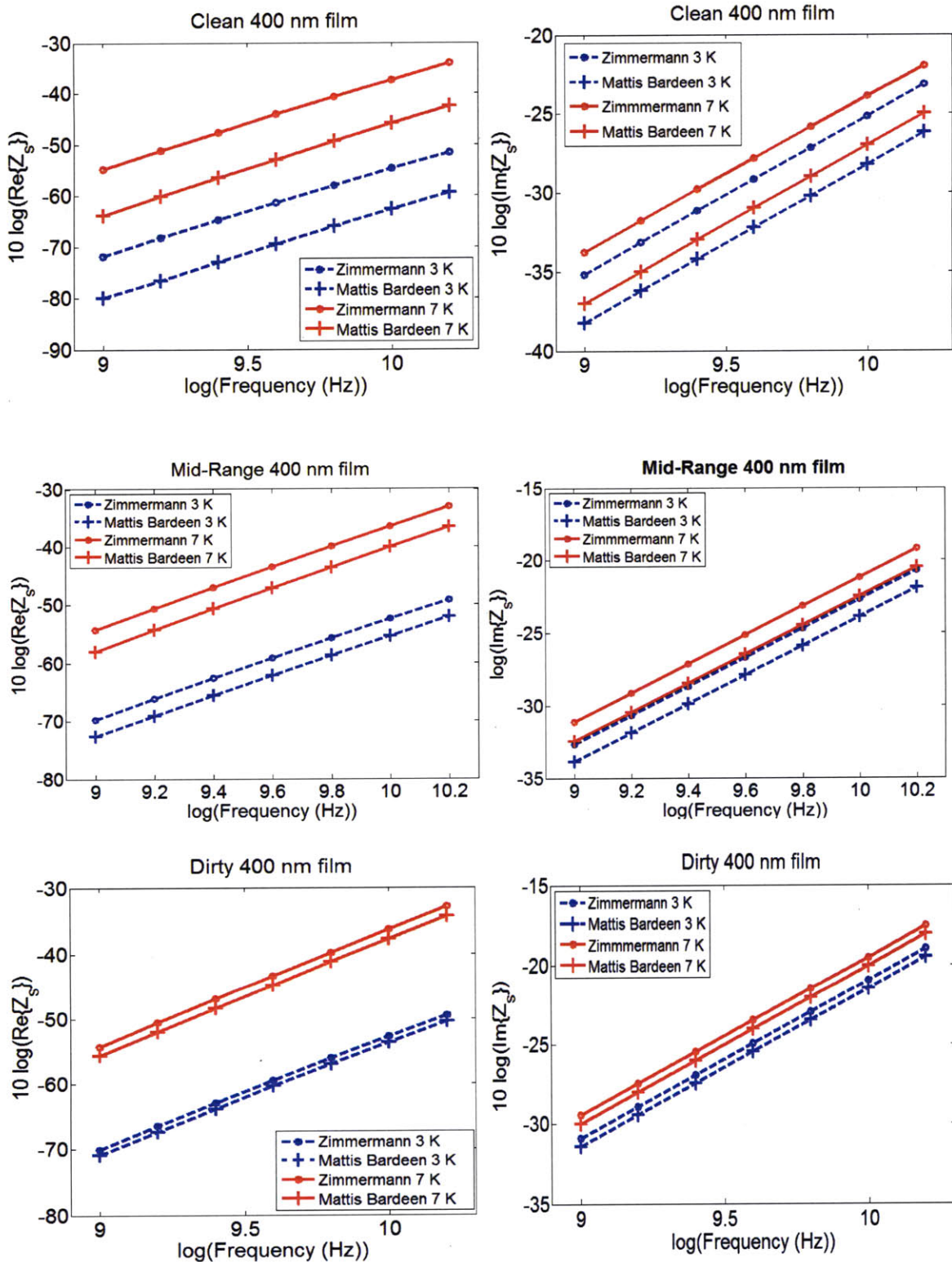
Figure 3-5: Plots of surface impedance of niobium films with parameters as given in Table 3-1. Red solid lines represent the calculations at 7K and blue dashed lines represent calculations at 3K. Circles –o– represent calculations done with the Zimmermann conductivity and crosses + represent calculations done with the Mattis Bardeen conductivity.

4 Simulation Results

The theory developed in Chapters 2 and 3 was applied to simulations of grounded coplanar waveguide resonators using Ansoft's HFSS 3D full-wave electromagnetic field simulation tool. This chapter will describe the simulation setup in HFSS and the software written to generate frequency-dependent surface impedance values for given material parameters.

This thesis contributes to a research effort aimed at developing high Q resonators for quantum computing applications. Adam McCaughan fabricated the prototype resonators throughout this project and reported his experimental method and results in [17]. Here, we will use the sets of dimensions which were used as fabrication prototypes to simulate the microfabricated niobium resonators.

In order to fully validate the proposed simulation technique for superconductors, we must compare simulation results against measured data. To do this accurately, we require knowledge of all material parameters of the niobium used to fabricate the resonator (its gap ratio, transition temperature, coherence length and either its normal state conductivity or its mean free path) as well as an accurate measurement of the temperature at which the data was taken. Such measurements are not currently available, but will be the next step in further work.

However, even without full knowledge of the superconductor parameters and precise temperature measurements, it is still possible to verify that the simulator predicts the expected trends in the variation of Q with parameters such as temperature and capacitive coupling, and generates the correct form of electric field distribution. We can also check that the Q's produced by the simulated resonators are reasonably close to those reported in [17], allowing, of course, for errors due to the uncertainty as to the superconductor parameters. Further, we can apply the simulator to a normal metal – thus eliminating the need for knowledge of any material parameter

other than normal state conductivity – and compare the results to measured data so as to verify that the classical transmission line theory basis of this tool is sound.

This chapter will report simulation results for both a printed circuit board (PCB) resonator and a microfabricated niobium-sapphire resonator.

4.1 Simulation Setup in HFSS

The grounded coplanar waveguide (CPW) geometry was modeled in HFSS as shown in Figure 4-1. In order to limit the solution space, the entire geometry was surrounded by an empty box with each face set as a radiation boundary and placed at a distance of 1/3 of the wavelength of the radiation (≈30mm) away from the resonator. Since we are simulating a *grounded* CPW, the top and bottom ground planes were shorted all around the CPW's edges by a perfect-E boundary condition. The power is delivered by lumped ports, shown in red in Figure 4-1.

Surface impedance boundary conditions were implemented in HFSS by representing the each conductor as an empty box and assigning a frequency-dependent impedance boundary condition to the top and bottom surfaces with the real and imaginary parts defined by calculated datasets of $Re(Z_s)$ versus frequency and $Im(Z_s)$ versus frequency. The calculation of these datasets was performed by MATLAB routines discussed in the next section.
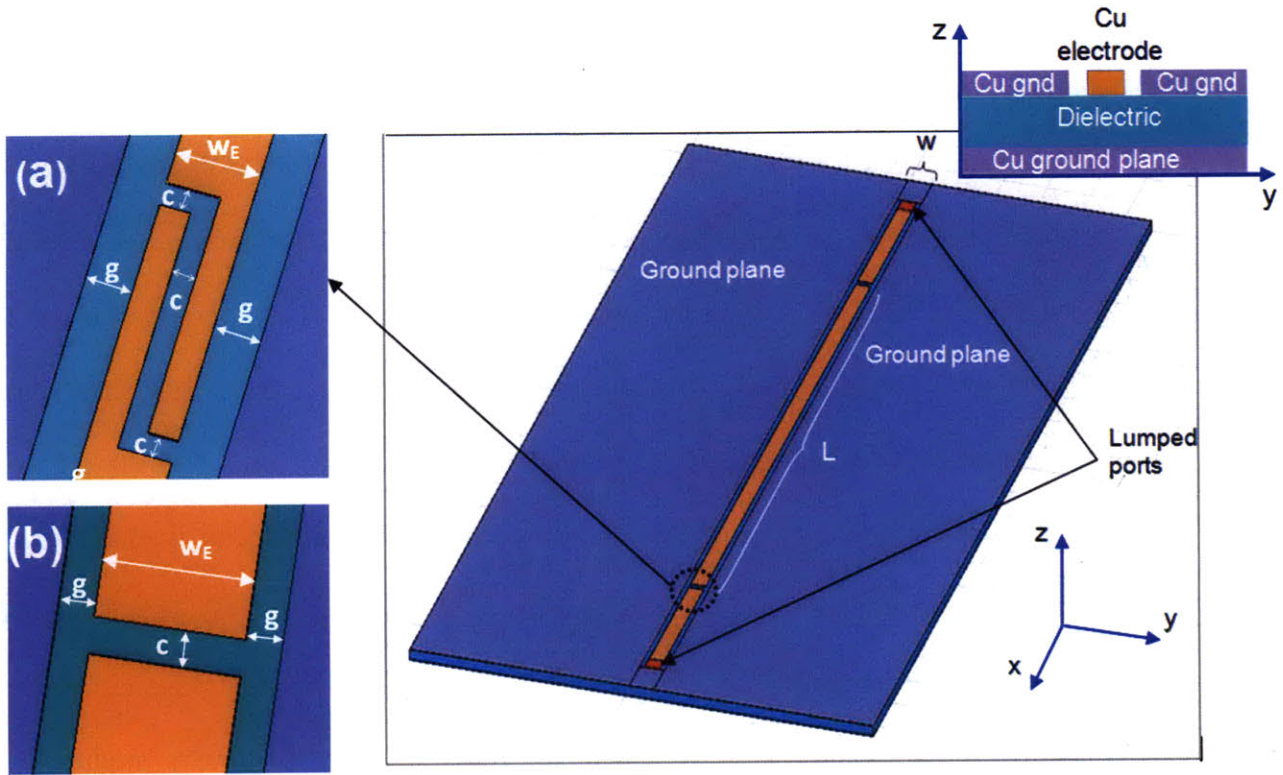
Figure 4-1: Grounded coplanar waveguide geometry in HFSS. Insets (a) and (b) show two different coupling capacitor configurations that will be simulated in throughout this chapter: (a) is a parallel gap capacitor and (b) is a fingered capacitor which gives a stronger coupling to the resonator for the same capacitive gap c. L denotes the length of the center electrode, w_E denotes the width of the center electrode, w denotes the total width of the electrode plus the gaps to the ground planes g.

4.2   Surface Impedance and Q-fitting Software

Surface Impedance Calculation

To generate the surface impedance datasets required by HFSS, the conductivity of the conductor or superconductor was computed and used to calculate the surface impedance with the formulae given in Chapter 2. However, before generating a dataset, one must consider:

1. Whether to use the Mattis Bardeen conductivity or the Zimmermann conductivity to calculate surface impedance. Recall from Chapter 3 that the Mattis Bardeen conductivity is only applicable for very dirty superconductors, with $l \approx 5$ nm.

2. Whether to calculate the bulk surface impedance, the surface impedance for a conductor of finite thickness for a one-sheet model of a conductor, or the corrected surface impedance for a two-sheet model of a conductor of finite thickness. Recall from Chapter 2 that the surface impedance of a conductor of thickness of the order of the skin depth is different from the bulk surface impedance. Recall also that, if one is applying a two-sheet model of a conductor, the surface impedance of each sheet must be a corrected Z_x (equation (2-8)) to account for the inductance seen between the two sheets. This correction is negligible if the thickness of the conductor is much larger than the skin depth, in which case Z_x reduces to Z_s as given in (2-4). It is of course valid to always compute the corrected Z_x for each sheet in the two-sheet finite-thickness model regardless of the metal thickness since it will always produce the correct surface impedance, reducing to the bulk Z_s (2-2) for very thick conductors.

Several MATLAB routines were written to produce the required datasets. All routines are printed in Appendix A and Table 4-1 gives a summary of their functions (parameter symbols defined in the caption).

Q-fitting Routine

A routine named *findQ.m* was developed to find Q given any S21 spectrum in dB. Following Petersan and Anlage [16], the routine converts the dB values to voltage ratios and fits this data with a modified Lorentzian (4-1), with coefficient p_5 accounting for any DC baselines and coefficient p_6 accounting for the possibility of a skew due to measurement problems.

$$f(\omega) = \frac{p_5 + p_4\omega + (p_3 + p_6\omega)}{\sqrt{1 + 4\left(\frac{(\omega - p_1)}{p_2}\right)^2}}$$ (4-1)

where ω is the frequency in GHz. The routine also calculates and prints the mean squared error

of the fit, which was consistently below 10^{-8} for the fitted simulation results. An example of a

set of simulation data fitted by the program is given in Figure 4-2.

Routine Name	Function	Required Input Parameters
Supercond.m	Calculates the ratio of the Mattis Bardeen conductivity to the normal state conductivity.	w, T, del0ratio,
Zimcond.m	Calculates the ratio of the Zimmermann conductivity to the normal state conductivity.	w, T, Tc, del0ratio, xi0, l
Rhonorm.m	Calculates the normal state conductivity from material parameters using equation (3-6).	Tc, del0ratio, xi0, l, LambdaL
Gap_supcond.m	Linearly interpolates a table of values of $\Delta(T)$ measured by Mühlschlegel [13] to find the energy gap at any temperature.	x = T/Tc
BulkZs.m	Calculates the bulk surface impedance from the conductivity using equation (2-2).	w, T, sn, rho0
FilmZs.m	Calculates the corrected surface impedance Z_x to be assigned to each sheet in the two-sheet model of a finite-thickness conductor the conductivity using equation (2-4).	w, T, sn, d, rho0

Table 4-1: Table of routines used to calculate surface impedance datasets. Parameter symbols: w = frequency; T=temperature; Tc = Transition temperature; xi0 = coherence length; l = mean free path; del0ratio=$\Delta(0)$/k_BTc where $\Delta(0)$ =energy gap at zero temperature; lambda = London depth; sn=normalized conductivity (i.e. ratio of Zimmermann or Mattis Bardeen conductivities to the normal state conductivity), rho0 = normal state resistivity
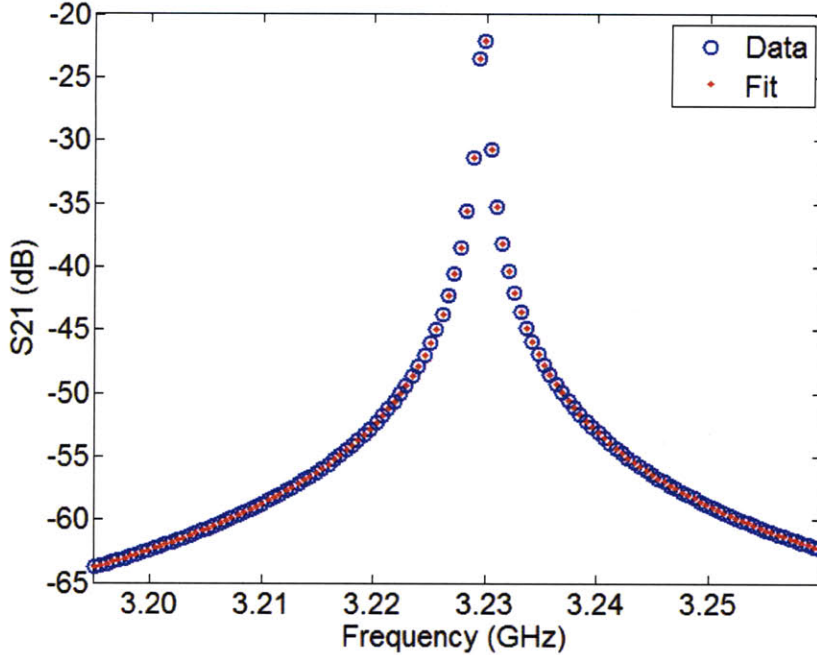
Figure 4-2: Example of a fitted set of simulation data using *findQ.m*. Here, Q = 9464, error =1.64 $\times$ 10^{-12}.

4.3   PCB Resonator

As an initial test of the HFSS resonator design and of the soundness of the transmission line theory used to develop the MATLAB surface impedance calculators described in the previous section, a PCB resonator was modeled with dimensions $w = 67$ mil and $L = 665$ mil, $w_E = 45$ mil, $g = 11$ mil, $c = 11$ mil (notation as defined in Figure 4-1). The resonator had the parallel gap coupling capacitor configuration of Figure 4-1 (b). The thickness of the copper on the PCB was 2.75 mil and the dielectric, Rogers RO4350™, was 30 mil thick. Figure 4-3 compares the measured [17] S21 spectrum to results for two simulation approaches: the green line is obtained when all copper surfaces are simply modeled as blocks which are assigned material "copper" from the HFSS materials library and the red line is produced when the center electrode is modeled as two sheets with surface impedance as calculated with *filmZs.m* (using the same conductivity value for copper as is listed in the HFSS materials library). The surface

impedance approach shows better agreement with the data because it accounts for the fact that the copper has finite thickness whilst HFSS most likely uses the bulk surface impedance for copper – note that the HFSS results give higher S21 values at each frequency: there is less power loss, which is consistent with the assumption of a thick conductor with lower resistance. The simulator does offer the option of solving for fields inside the conductor to obtain an accurate solution, but this is precisely what we were trying to avoid in developing the theory in Chapter 2.
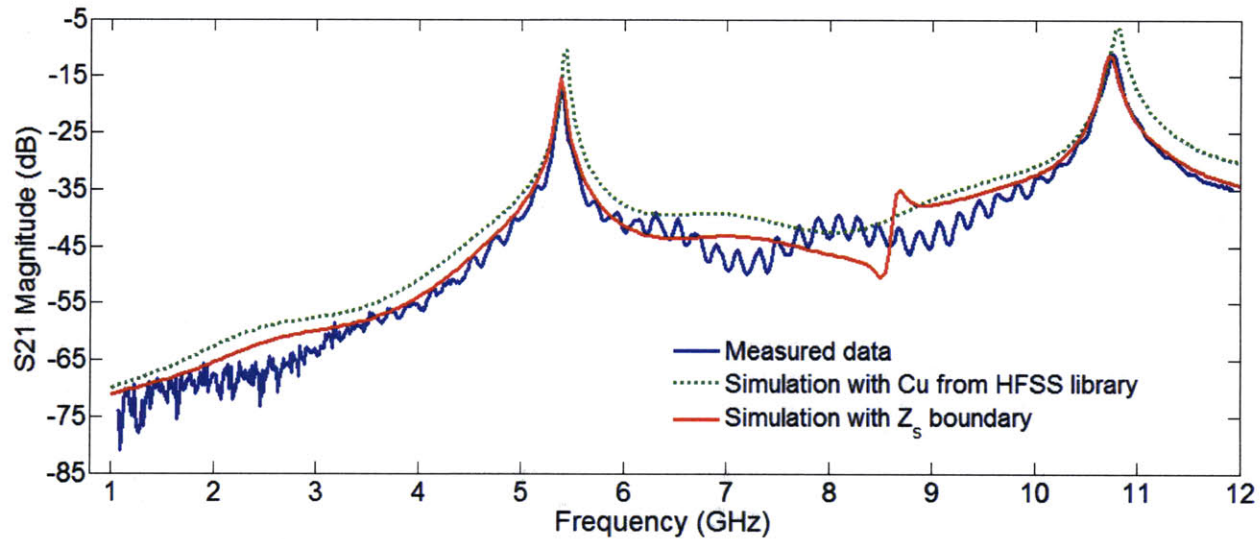

Figure 4-3: Simulation results compared to measured data (jagged blue line) for the PCB grounded coplanar waveguide resonator. The solid red line indicates the results obtained when two sheets of the appropriate surface impedance Z_s are used to model the center electrode and the dotted green line is obtained when we the electrode is represented by a box filled with the material "copper" as selected from the HFSS materials library. The surface impedance model is in better agreement with measured data.

4.4   Niobium Resonator

Using the Zimmermann conductivity in *filmZs.m*, we were able to calculate the surface impedance for a superconductor of arbitrary purity. We were also able to calculate the surface impedance at any temperature using the both the Mattis Bardeen and Zimmermann conductivities for dirty superconductors, and the Zimmermann conductivity for clean superconductors. If we then apply these surface impedances in simulation, we can generate Q values for any temperature and mean free path, given the material parameters.

Figure 4-4 plots Q versus temperature for the dirty niobium listed in the last column of Table 3-1 using the Mattis Bardeen conductivity. The simulations for this plot were run with a niobium-sapphire resonator with dimensions $w = 38$ μm and $L = 19.937$ mm, $w_E = 18$ μm, $g = 10$ μm, $c = 5$ μm (notation as defined in Figure 4-1). The resonator had the fingered coupling capacitor configuration of Figure 4-1 (b) with fingers of length 54 μm and width 6.5 μm. The thickness of the niobium was 400 nm and the sapphire was 0.33 mm thick and had relative permittivity 9.3. We see from the plot that, as expected, Q decreases with increasing temperature due to an increase in surface resistance, which is shown in Figure 3-4. We also see that the Q's obtained at the likely operating temperatures of 1K to 3K are within tens of percent of those reported by McCaughan [17].
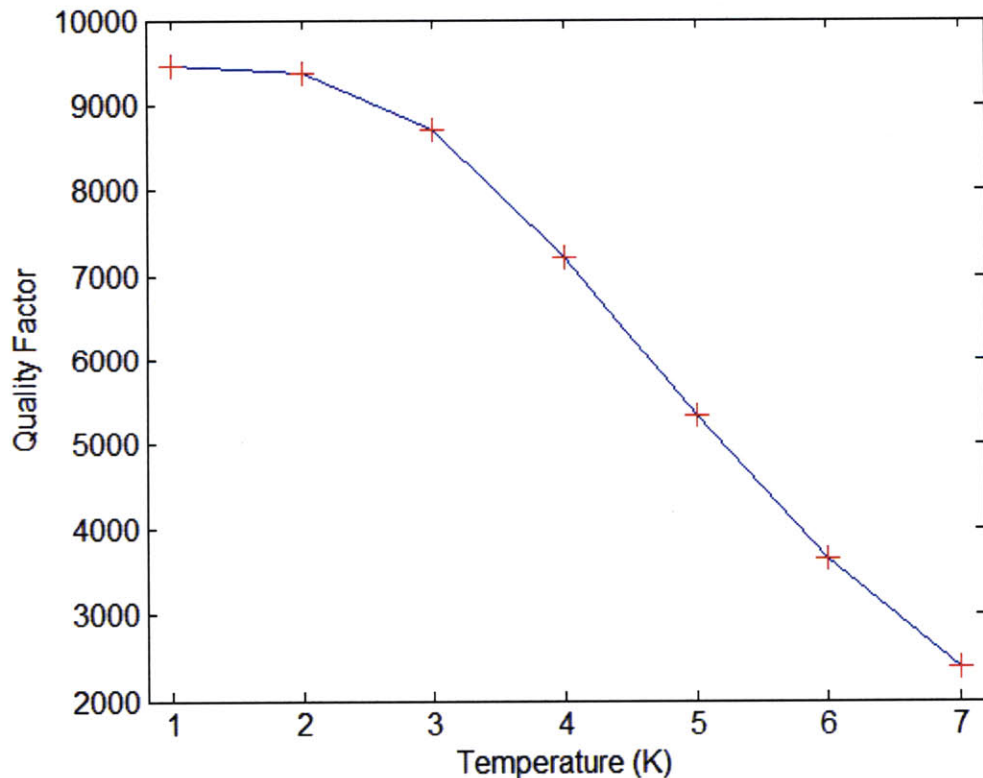

Figure 4-4: Plot of Q versus temperature obtained by applying a surface impedance as calculated by *filmZs.m* with the Mattis Bardeen conductivity to the HFSS simulation. The niobium simulated here is the "dirty" niobium with parameters listed in the last column of Table 3-1.

In order to match experiment to simulation, it is important to recall that any coupling capacitance or mismatched impedance introduced by the measuring equipment (for instance, a small gap between part of the network analyzer probe and the input port of the resonator) which is not modeled exactly in simulations will introduce very large variations in loaded Q. Goeppl [19], shows, for example, that if the coupling capacitance of his Aluminum CPW's increases from 0.4pF to 56pF, the Q decreases from 200,000 to 370.

In order to accurately compare simulation and measurement, therefore, it is necessary to determine the unloaded Q. This can be done by taking into account the coupling capacitance of the resonator, or by increasing the capacitive gap until the Q saturates at a capacitance-independent value – once the Q begins to vary negligibly with capacitance, we are in the *under-coupled* regime.

Figure 4-5 shows the variation of Q when the capacitive gap is increased from 5 to 20 μm in a resonator with a parallel gap coupling capacitor (and with otherwise the same parameters listed earlier in this section) simulated using the Zimmermann conductivity. We see that the Q increases as the gap increases (and the coupling capacitance decreases), but the increase is very small – of the order of 2%. This implies that we are in the under-coupled regime and that the Q determined here is very close to the unloaded Q. These results are consistent with Goeppl's [19] measurements in the under-coupled regime – over a 20 μm change in gap, he reports no significant change in Q.

Figure 4-6 plots Q versus mean free path using the Zimmermann conductivity at 3K for the same resonator geometry as described for Figure 4-4. We discover an interesting result: the cleaner the superconductor, the lower the Q it produces. To fully understand this

effect, it would be useful to develop an analytical model which allows for the calculation of Q directly from values of surface resistance and surface reactance – a possible approach to this is discussed in chapter 5.
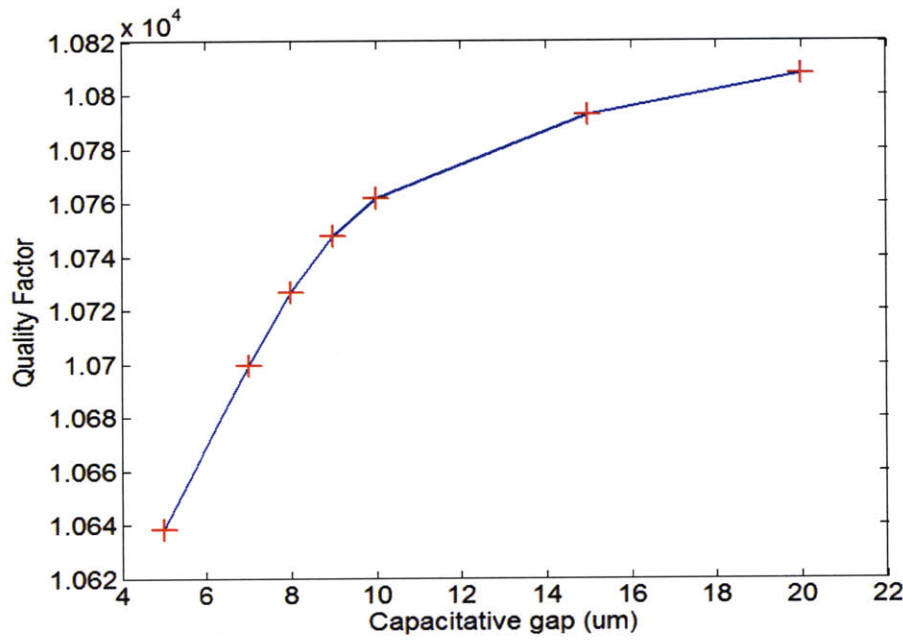
Figure 4-5: Plot of Q versus capacitive gap for a Nb resonator where the Nb has $l = 10$ nm and is at a $T = 1$K.
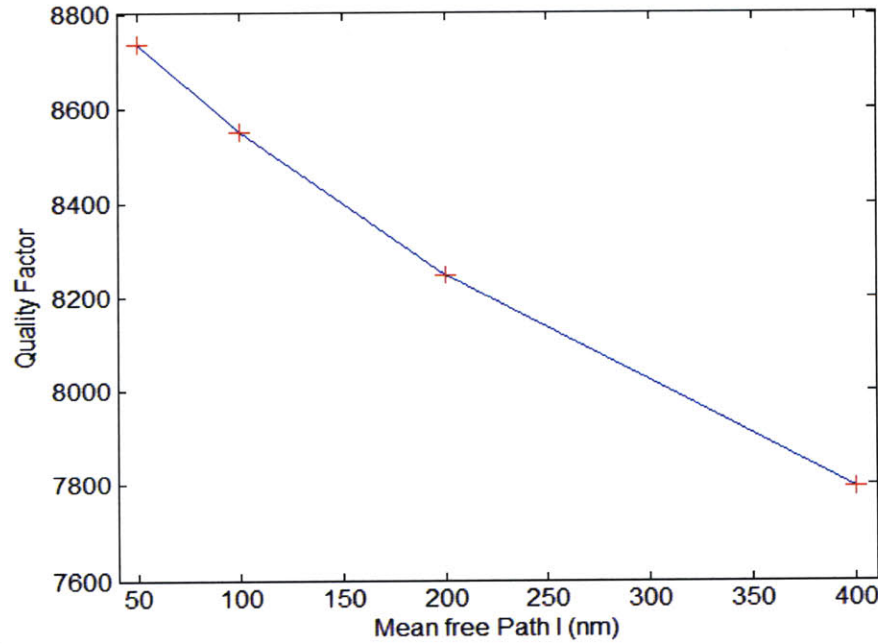
Figure 4-6: Plot of Q versus mean free path length l at temperature $T = 3$K obtained by applying using the surface impedance boundary condition calculated by *filmZs.m* with the Zimmermann conductivity to the HFSS simulation. The Mattis Bardeen conductivity is not used here since, as we saw in Chapter 2, it is only applicable for very small mean free path $l \approx 5$nm.

It is interesting to note here that, not only can we predict the Q given the material parameters, but, if we have one unknown material parameter and can measure the Q, we are able to determine that parameter by matching simulations to measured data. It is possible therefore to determine the mean free path of a sample if the measurement temperature is known, or, similarly, to determine temperature if sample purity is known.

To conclude this section, we show the tremendous increase in Q which arises from the use of a superconductor instead of a normal metal in the microfabricated resonator. Figure 4-7 shows simulation results when niobium is replaced by Silver, a metal with an excellent normal state conductivity of $61 \times 10^6 S/m$.
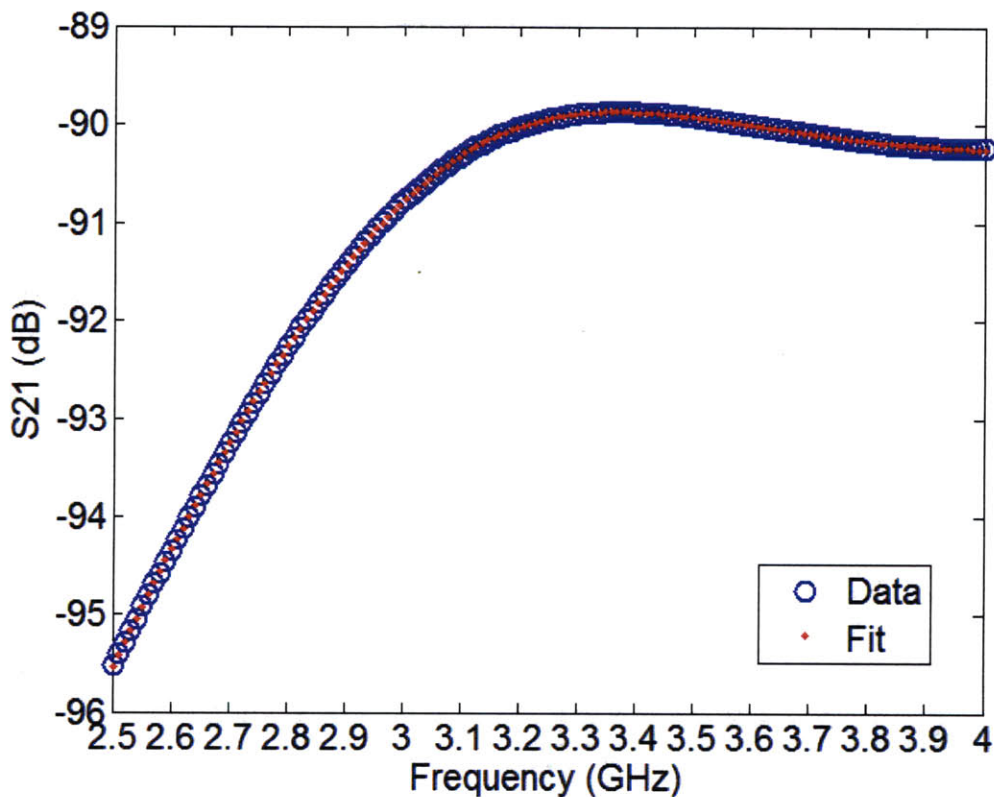

Figure 4-7: Simulated Q for microfabricated resonator with normal state Silver in place of a superconductor. Here $Q = 2.42$, a thousand-fold decrease from the superconducting Q's for the same resonator seen in Figure 4-4 and **Error! Reference source not found.**.

4.5   Electric Fields

For quantum computing applications, we are interested in the second resonance of the S21 spectrum, where the standing wave on the resonator electrode consists of one full wavelength and the field at the center of the electrode is at a maximum, as required for ion trapping (Figure 4-8). Figure 4-9 and Figure 4-10 are plots of the electric field obtained by modeling all niobium surfaces of the microfabricated grounded coplanar waveguide as two sheets with surface impedance as calculated by *filmZs.m* using the Zimmermann conductivity, at a temperature of 1K for a niobium with mean free path of $l = 10$ nm and a the gap ratio equal to the BCS value of 1.76. The resonator geometry used here is the same as described for Figure 4-4 but with a butted capacitance with a capacitive gap $c = 5$ μm.
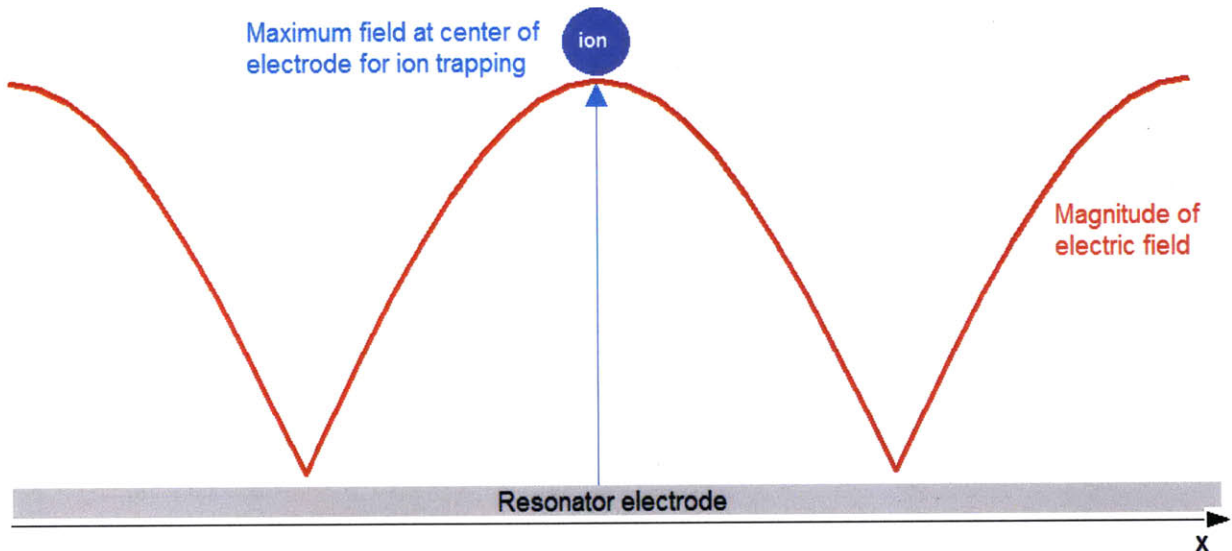
Figure 4-8: Schematic diagram of field along center electrode (X axis as defined in Figure 4-1) for the second resonance (≈6GHz). This resonance provides a field maximum at the center of the resonator, which is required for ion trapping.
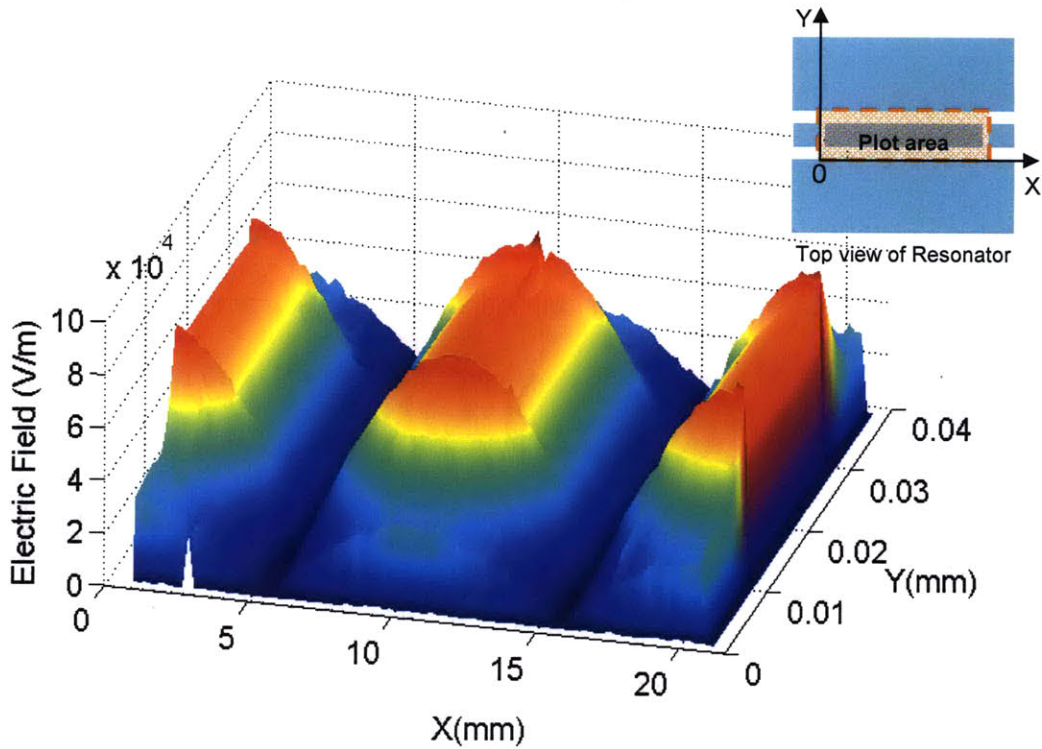
Figure 4-9: Plot of electric field over the surface of CPW, at a distance of 38μm above the resonator. The second harmonic standing wave with two nodes and a central maximum is clearly visible here and, as expected, the field is constant over the electrode, spikes at the edges and decays over the gaps between the electrode and the ground planes.
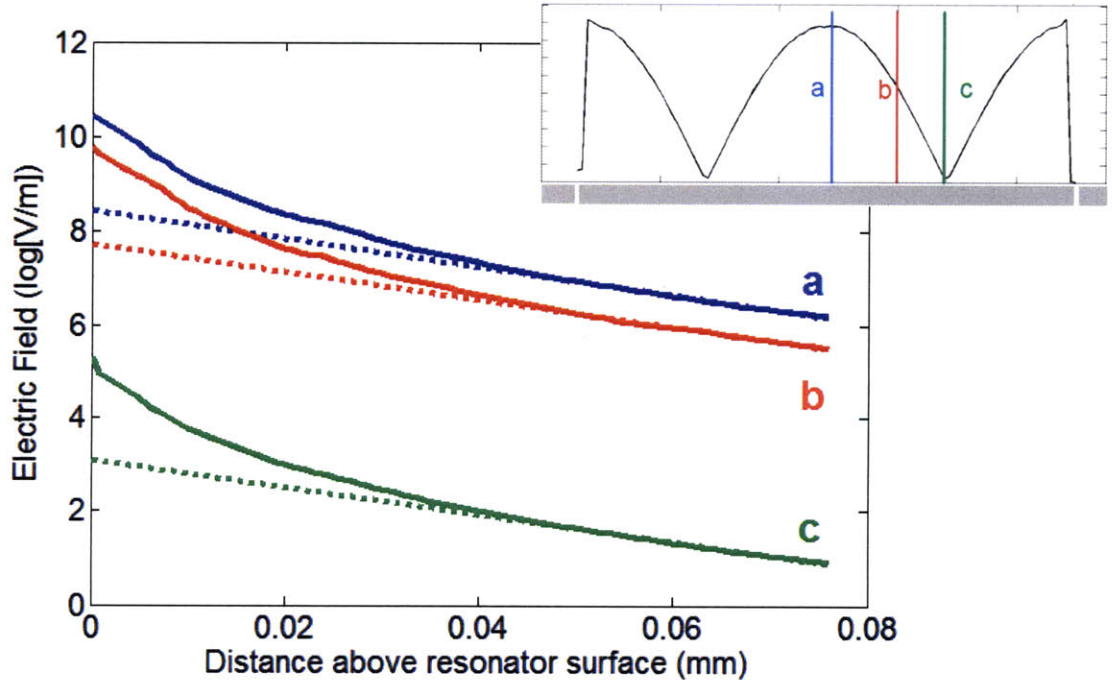
Figure 4-10: Logarithmic plot of electric field at different distances along the central resonator electrode. Apart from slight deviations close to the surface of the resonator (which can be attributed to meshing artifacts or near-field effects), the field decay is exponential and extrapolated linear fits (dotted lines) can be used to establish the field at ion-trapping distances above the surface.

As we can see from the field plots, the electric field distribution predicted by the simulator is qualitatively correct. Quantitative experimental verification of field simulation results for any known set of material parameters could be obtained using a spectroscopy setup such as is described in [19] as follows: a Sr^+ ion is trapped above the resonator (which is integrated into a cryogenically operated Paul trap [3]) and a magnetic field in applied to produce Zeeman splitting of its hyperfine levels. The electric field will generate Rabi oscillations between the Zeeman states and the frequency of these oscillations will be proportional to the magnitude of the electric field at the ion's location in space. Therefore, the field can be mapped by moving the ion across the surface of the resonator (which can be accomplished by changing electrode potentials of the Paul trap) and recording the Rabi frequency at several locations.

5 Conclusions and Further Work

This thesis develops a simulation tool which, when used with commercially available electromagnetic simulators, can model the behavior of superconductors of arbitrary purity over a wide range of frequencies, predicting Q factors, electric field distributions and S21 transmission spectra for superconducting devices. This simulator can also be used to generate a table of values of Q for a given device geometry as a function of metal purity (mean free path) and operating temperature. If one then takes a superconductor of unknown purity, measures its gap ratio, transition temperature, and the Q produced when it is used to make the given device, it is possible to use this tool to determine the superconductor's mean free path by comparing measured data with simulation results. If all material parameters are known, it is also possible to determine the temperature at which the Q measurements were made.

Simulation results for a printed circuit board resonator were an excellent match to measured data, confirming the soundness of the transmission line theory basis of this simulator, as developed in Chapter 2. When a microfabricated niobium resonator was modeled, the obtained variation of Q with temperature and capacitive coupling followed the expected trends, and, allowing for errors due to the lack of information about the superconductor's parameters, the Q's obtained were in good agreement with measured data (within tens of percent). The simulated distribution of the electric field over the resonator was also of the correct form.

The next step in further work will be to measure the Q of a resonator fabricated with a niobium sample of known material parameters and compare it with simulated results. In performing the measurements, one can either compare loaded Q simulation to measurement using a very well controlled measurement setup where all coupling capacitances are known and can be simulated exactly (such as the measurement setup shown in [20]), or one can determine

unloaded Q by decreasing the coupling capacitance to the device until the measured Q saturates at a constant value. The unloaded Q can then also be determined from simulation by taking capacitance into account, as shown in Chapter 3.

It would be interesting to pursue, in further work, the development of an analytical model which allows for the calculation of Q directly from values of surface resistance and surface reactance. This could perhaps be accomplished by running simulations with resonators of different lengths (and hence different surface areas) and determining the dependence of Q and resonant frequency on surface resistance and reactance. Using a simple *RLC* model for the resonator, one may be able to establish how much of the lumped resistance, inductance and capacitance is derived from surface effects and how much is due to the intrinsic transmission line impedance.

Another goal for future work is to use this tool to establish ways of increasing the Q by changing the resonator design.

The tool developed here can be used to optimize and characterize superconducting devices, avoiding the need for repetitive and costly fabrication and measurement cycles.

References

1. **Ward, J., Rice, R., Chattopadhyay.** SuperMix: a flexible software library for high-frequency circuit simulation, including SIS mixers and superconducting elements. *Proc. Tenth International Symposium on Space Terahertz Tech.* 1999, Vols. pp 269-281.

2. **Chiaverini, J. et al.** *Quant. Inf. Comput.* 5419, 2005.

3. **Antohi, P.B., et al.** Cryogenic Ion Trapping Systems with Surface-Electrode Traps . *Rev.Sci.* 2009, Vol. 80, 013103.

4. **Kerr, A. R.** Surface Impedance of Superconductors and Normal Conductors in EM Simulators. *MMA Memo No.245 - NRAO Electronics Division Internal Report No.302.* 1999.

5. **Pozar, D.M.** *Microwave Engineering.* s.l. : John Wiley & Sons, Inc., 2005.

6. **Matick, R.E.** *Transmission Lines for Digital and Communication Networks.* s.l. : McGraw-Hill, 1969.

7. **Kittel, C.** *Introduction to Solid State Physics.* s.l. : John Wiley & Sons, 2005.

8. **Bardeen, J., Cooper, L.N., Schrieffer, J. R.** Microscopic Theory of Superconductivity. *Phys. Rev.* 1957, Vol. 106.

9. **Linden, D., Orlando, T.P., Lyons, W.G.** Modified Two-Fluid Model for Superconductor Surface Impedance Calculation. *IEEE Transactions on Applied Superconductivity.* 1994, Vol. 4, 3.

10. **Mattis, D.C., Bardeen, J.** Theory of the Anomalous Skin Effect in Normal and Superconducting Metals. 111, 1958, Vol. 412.

11. **Gao, J.** *The Physics of Superconducting Microwave Resonators.* s.l. : California Institute of Technology Ph.D. Thesis, 2008.

12. **Glover, R.E., Tinhham, M.** Conductivity of Superconducting Films for Photon Energies between 0.3 and 40kTc. *Physics Review.* 108, 1957, Vol. 243.

13. **Muhlschlegel, B.** Die thermodynamischen Funktionen des Supraleiters. *Zeitschrift für Physik.* 155, 1959, Vol. 313.

14. **Zimmermann, W. et al.** Optical Conductivity of BCS superconductors with arbitrary purity. *Physica C.* 1991.

15. **Linden, D.** A Modified Two-Fluid Model for Superconducting Surface Resistance Calculation. *Massachusetts Institute of Technology PhD thesis.* 1993.

16. **Petersan, P.J., Anlage, S.M.** Measurement of Resonant Frequency and Quality Factor of Microwave Resonators: Comparison of Methods. *Journal of Applied Physics.* 1998, Vol. 84.

17. **McCaughan, A.N.** *MIT Meng Thesis.* 2010.

18. **Goppl, M., et al.** CoPlanar Waveguide Resonators for Circuit Quantum ElectroDynamics. *Journal of Applied Physics.* 2008, Vol. 104.

19. **Labaziewicz, J.** *High Fidelity Quantum Gates with Ions in Cryogenic Microfabricated Ion Traps.* s.l. : Massachusetts Institute of Technology Ph.D. Thesis, 2008.

20. **Frunzio, L., et al.** Fabrication and characterization of superconducting circuit QED devices for quantum computation. *IEEE trans. Appl. Supercond.* 2005, Vol. 15.

21. **Reuter, G.E., Sondheimer, E. H.** The Theory of the Anomalous Skin Effect in Metals. *Proc. Roy. Soc. (London).* 1948, Vol. A195.

Appendix A : MATLAB Routines

A1.   Supercond: Mattis Bardeen conductivity calculator

```
function sigma_ratio = supercond(w, T, sup)
% supercond(w, T, sup)
% Computes the complex conductivity ratio of a
% superconductor sup at angular frequency w and temperature T.
% This is done by numerically integrating the Mattis Bardeen
% equations.

% Get required superconductor characteristics
Tc = sup.Tc;
del0ratio = sup.del0ratio;

kb = 1.3806503e-23;       % Boltzmann constant
hbar = 1.054571628e-34;   % reduced Planck constant

del0 = del0ratio*kb*Tc;  % delta at 0 K
delt = gap_supcond(T/Tc)*del0; % temperature corrected delta

if (w > (2*delt/hbar))
    fprintf('Warning: w too large in function supercond\n');
end

% Computes the conductivity ratio by numerical integration.
% First find a reasonable upper limit to replace infinity in
% the first integral (was fixed at 1.5e11*delt). The algorithm
% used works well provided the temperature is not too near Tc or 0 K.

if (T<0.5) | (T>8.5)
    fprintf('Warning: results may not be accurate at this temp.\n');
end

if T>7.8
    upper_limit = delt*(1.3*T/1.5 - 4.617)*1.3e11;
else
    upper_limit = delt*(1.5*T/6 + 0.225)*1e11;
end

sigma1Lint=quad('sigma1L',0,upper_limit,1e-4,0,w,T,delt);
sigma2Lint=quad('sigma2L',0,sqrt(hbar*w/2),1e-4,0,w,T,delt);
sigma2Uint=quad('sigma2U',0,sqrt(hbar*w/2),1e-4,0,w,T,delt);
sigma_ratio = sigma1Lint - j*(sigma2Lint + sigma2Uint);
```

```
function y = sigma1L(x, w, T, delt)
% sigma1L(x, w, T, delt)
% Integrand used to find the real part of the complex conductivity
% E -> delt + x^2 (to remove the square root singularity at the lower limit)
% new lower limit = 0; new upper limit = Inf
E = delt + x.^2;
hbarw = w*1.054571628e-34;
```

```matlab
y = (4/hbarw)*(fermi(E, T) - fermi(E + hbarw, T)).*(E.^2 + delt^2 +
hbarw*E)./(sqrt(2*delt + x.^2).*sqrt((E + hbarw).^2 - delt^2)));
```

```matlab
function y = sigma2L(x, w, T, delt)
% sigma2L(x, w, T, delt)
% Integrand used to find the imaginary part of the complex conductivity
% E -> delt - hbarw + x^2 (to remove the square root singularity at the lower
limit)
% new lower limit = 0; new upper limit = sqrt(hbarw)
hbarw = w*1.054571628e-34;
E = delt - hbarw + x.^2;
y = (2/hbarw)*(1 - 2*fermi(E + hbarw, T)).*(E.^2 + delt^2 +
hbarw*E)./((sqrt(delt^2 - E.^2).*sqrt(2*delt + x.^2)));
```

```matlab
function y = sigma2U(x, w, T, delt)
% sigma2U(x, w, T, delt)
% Integrand used to find the imag part of the complex conductivity
% E -> delt - x^2 (to remove the square root singularity at the upper limit)
% new lower limit = 0; new upper limit = sqrt(hbarw)
E = delt - x.^2;
hbarw = w*1.054571628e-34;
y = (2/hbarw)*(1 - 2*fermi(E + hbarw, T)).*(E.^2 + delt^2 +
hbarw*E)./((sqrt(2*delt - x.^2).*sqrt((E + hbarw).^2 - delt^2)));
```

A2.   Zimcond: Zimmermannn conductivity calculator

```matlab
function s = zimcond(w, T, sup)
% zimcond(w, T, sup)
% Computes the complex conductivity ratio of a
% superconductor sup at angular frequency w and
% temperature T using the Zimmermann method.

% Get required superconductor characteristics
Tc = sup.Tc;
del0ratio = sup.del0ratio;
xi0 = sup.xi0;
l = sup.l;

kb = 1.3806503e-23;       % Boltzmann constant
hbar = 1.054571628e-34;   % reduced Planck constant

del0 = del0ratio*kb*Tc;
delt = gap_supcond(T/Tc)*del0; % temperature corrected delta
k = del0/delt;

if (w > (2*delt/hbar))
    fprintf('Warning: w too large in function zimcond\n');
end

s = conj(zimcalc((hbar*w/2/delt), (pi/2)*(xi0/l)*k, T/Tc, del0ratio));
```

```
function s = zimcalc(x, y, tt, del0ratio)
% zimcalc(x, y, tt, del0ratio)
% Computes the complex conductivity of a superconductor using
% the Zimmermann et al approach.
% Inputs: x = hbar*w/(2*delta), y=hbar/(2*delta*tau), tt=T/Tc
% where w is the angular frequency, delta is the gap, Tc is
% the critical temp and tau is the electron collision time. If
% the electron mean free path is le and vf is the Fermi velocity
% tau = le/vf.  The coherence length xi0 = hbar*vf/(pi*delta0)
% so y can also be written y = (pi/2)*(xi0/le)*(delta0/delta).

deltratio = del0ratio*sqrt(1-tt)*(0.9963 + 0.7733*tt);
t = tt/(2*deltratio);
M = 250;
du = 1/M;
urange = 0.5*du:du:1;
s1 = sum(zimint1(urange, x, y, t));
s2 = sum(zimint2(urange, x, y, t));
s = (s1*du + s2*du)*j*y*0.5/x;


function int1 = zimint1(u, x, y, t)
% zimint1(u, x, y, t)
% Zimmermann integral 1
e = 0.5 + x*u.*u.*(3-2*u);
tiny = 1e-20;
small = 1e-3;
p4 = j*sqrt(0.25 - (e-x).^2);
p2 = sqrt(e.^2 - 0.25);
c42 = (0.25 + e.*(e-x))./(p4.*p2 + tiny);
cy = j*y;
th = tanh(e/(2*t + small));
int1 = 6*x*th.*((1-c42)./(p4+p2+cy) - (1+c42)./(p4-p2+cy)).*u.*(1-u);


function int2 = zimint2(u, x, y, t)
% zimint2(u, x, y, t)
% Zimmermann integral 2
e = 0.5 + (u./(1-u)).^2;
tiny = 1e-20;
small = 1e-3;
p1 = sqrt((e+x).^2 - 0.25);
p2 = sqrt(e.^2 - .25);
c12 = (.25 + e.*(e+x))./(p1.*p2 + tiny);
cy = j*y;
th1 = tanh((e+x)/(2*t + small));
th2 = tanh(e/(2*t + small));
int2 = 2*(th1.*((1+c12)./(p1-p2+cy) - (1-c12)./(-p1-p2+cy))...
    + th2.*((1-c12)./(p1+p2+cy) - (1+c12)./(p1-p2+cy))).*u./(1-u).^3;
```

A3.   Rhonorm: Normal resistivity calculator

```
function rho0 = rhonorm(Tc, del0ratio, lambdaL, xi0, l);
% rhonorm(Tc, del0ratio, lambdaL, xi0, l)
% Computes the normal resistivity (in ohm-m) of a superconductor
% based on its superconductivity parameters.

mu0=4*pi*1e-7;             % magnetic constant
kb = 1.3806503e-23;        % Boltzmann constant
hbar = 1.054571628e-34;    % reduced Planck constant

del0 = del0ratio*kb*Tc;
rho0 = lambdaL^2*mu0*pi*del0*xi0/(l*hbar);
```

A4.   Gap_supcond: Gap calculator from *SuperMix* [1]

```
function gap = gap_supcond(x)
% gap_supcond(x)
% Calculates superconducting energy gap as a function of temp
% ratio x = T/Tc.  (This function was taken from supermix.)

% Table of reduced energy gap vs. T/Tc, from Muhlschlegel (1959).
% Table starts at x = T/Tc = 0.18, and goes in steps of dx = 0.02

ratio = [
    1.0,
    0.9999,
    0.9997,
    0.9994,
    0.9989,
    0.9982,
    0.9971,
    0.9957,
    0.9938,
    0.9915,
    0.9885,
    0.985,
    0.9809,
    0.976,
    0.9704,
    0.9641,
    0.9569,
    0.9488,
    0.9399,
    0.9299,
    0.919,
    0.907,
    0.8939,
    0.8796,
    0.864,
    0.8471,
    0.8288,
    0.8089,
```

```matlab
   0.7874,
   0.764,
   0.7386,
   0.711,
   0.681,
   0.648,
   0.6117,
   0.5715,
   0.5263,
   0.4749,
   0.4148,
   0.3416,
   0.2436,
   0.0 ];

% check if x is physical

if (x < 0) | (x >= 1)
   gap = 0;
   return
end

if (x < 0.04)
   gap = 1;
   return
end

% if x <= 0.32, we use an analytic expression to extend the gap table;
% (which uses k Tc ~= Delta(0)/1.764; c.f. Tinkham)

xmatch = 0.32;   % xmatch must be a multiple of 0.02, >= 0.18
ymatch = exp(-sqrt((2*pi/1.764)*xmatch)*exp(-1.764/xmatch));

if (x <= xmatch)
   gap = exp(-sqrt((2*pi/1.764)*x)*exp(-1.764/x));
   return
end

% if we get here, we interpolate between data points to calculate gap, taking
% sqrt(1 - T/Tc) dependence near the gap into account.

index = floor((x-0.18)/0.02);   % index into ratio table
xl = index*0.02 + 0.18;
xu = xl + 0.02;

if (xl > xmatch)
   yl = ratio(index + 1)/sqrt(1-xl);   % Changed to account for Matlab
indexing
else
   yl = ymatch/sqrt(1-xl);
end

if (index < 40)
   yu = ratio(index + 2)/sqrt(1-xu);   % Changed to account for Matlab
indexing
```

```
else
    yu = 1.74;   % behavior near Tc - see Tinkham, eqn. 2-54.
end

gap =  sqrt(1 - x) * (yl + (yu-yl)*(x-xl)/(xu-xl));   % linear interp into
ratio table
```

A5.   BulkZs: Bulk surface impedance calculator

```
function Zs = bulkZs(w, sigma, sup)
% bulkZs(w, sigma, sup)
% Computes the bulk surface impedance at angular
% frequency w for a material sup with normalized
% conductivity sigma.

rho0 = sup.rho0;

mu0 = 4*pi*1e-7;
Zs = sqrt(j*w*mu0/(sigma/rho0));
```

A6.   FilmZs: Finite thickness surface impedance calculator

```
function Zx = filmZs(w, sn, d, sup)
% filmZs(w, sn, d, sup)
% Computes the surface impedance of a sup film of thickness
% d with normalized conductivity sn at angular frequency w.
% Includes the inductance correction for the two sheet model.

rho0 = sup.rho0;

mu0=4*pi*1e-7;        % magnetic constant
sigma0 = 1/rho0;      % normal conductivity
Zn = 376.730313;      % impedance of free space
c = 299792458;        % speed of light in vacuum

s1 = sn*sigma0;
delta = sqrt(2/(mu0*w*s1));
lambda2 = (1 + j)/delta;
L = Zn*tan(w*d/c)/w;

% Compute the surface impedance - classical Zs from Matick pg 128
Zs = (lambda2/s1)*coth(lambda2*d);

% Correction using the inductance between two sheets = L
Zx = 0.5 *((2*Zs - j*w*L) + sqrt(4*Zs^2 +(j*w*L)^2));
```

A7. FindQ: *Q* calculator

```
% Find Q from S21 data.
%
% According to Petersan and Anlage, "Measurements of Resonant frequency
% and Quality Factor of Microwave Resonators: Comparison of Methods"
% (http://arxiv.org/pdf/cond-mat/9805365), a good way to find Q is to
% fit a Lorentzian curve to the measurement data.  This program does
% that using Matlab's non-linear least squares fitting routines.

% Input should be an ASCII data file with frequency as the first column
% and measured power (in dB) in the second column. Frequency is assumed
% to be of order 1e9.

clear
close all
clc

% load measured data
S21 = load('S21.txt');
x = S21(:,1)/1e9;   % scale frequency
measured = S21(:,2);
y = 10.^(measured/20);

plot(x,measured,'bo'); % show measured data
hold on;

% esti
[peak ipeak] = max(y); % guess the gain
fres = x(ipeak);        % guess the resonant frequency
N = size(x);

% find approx half power index
ihalf = 0;
for i = ipeak:N,
    if (y(i) <= peak/sqrt(2))
        ihalf = i;
        break
    end
    i = i + 1;
end

Q = 1000;
if ihalf > 0
    Q = fres/2/(x(ihalf) - fres);  % guess Q
end

p0 = [fres fres/Q peak 0.000001 0.1 0.0001];  % starting parameters

guess = lorentz_model(p0, x); % show inital guess
plot(x,20*log10(guess),'r-');


% improve the guess by fitting
```

```matlab
p1 = nlinfit(x, y, @lorentz_model, p0);
p2 = lsqcurvefit(@lorentz_model, p0, x, y);

% show fitted curves
y1 = lorentz_model(p1, x);
plot(x,20*log10(y1),'g.');
y2 = lorentz_model(p2, x);
% plot(x,20*log10(y2),'g-');
legend('Data', 'Fit');
xlabel('Frequency (GHz)');
ylabel('S21 (dB)');

e1 = sum((y-y1).^2);
e2 = sum((y-y2).^2);
fprintf('          Guessed: Peak = %f, Resonant freq = %f, Q = %f\n', peak, fres, Q);
fprintf('NLINFIT Estimated: Peak = %f, Resonant freq = %f, Q = %f (error = %.2e)\n', p1(3), p1(1), abs(p1(1)/p1(2)), e1);
fprintf('LSQCFIT Estimated: Peak = %f, Resonant freq = %f, Q = %f (error = %.2e)\n', p2(3), p2(1), abs(p2(1)/p2(2)), e2);
```